Dissecting the interstellar medium of a z=6.3 galaxy.

X-shooter spectroscopy and HST imaging of the afterglow and environment of the Swift GRB 210905A

Stargate Collaboration

ANDREA SACCARDI

2nd year PhD Student

Observatoire de Paris - GEPI

Supervisor: S.D. Vergani

HIGH REDSHIFT GAMMA-RAY BURSTS IN THE JWST ERA

9-13 January 2023 - Sexten

SEXTEN CENTER FOR ASTROPHYSICS RICCARDO GIACCONI

Credits: Futura Science

Major issues of extragalactic astronomy

-What are the first objects to be formed in the Universe?

-How do galaxies form and evolve?

-What is the interplay between star formation and the inter-stellar gas?

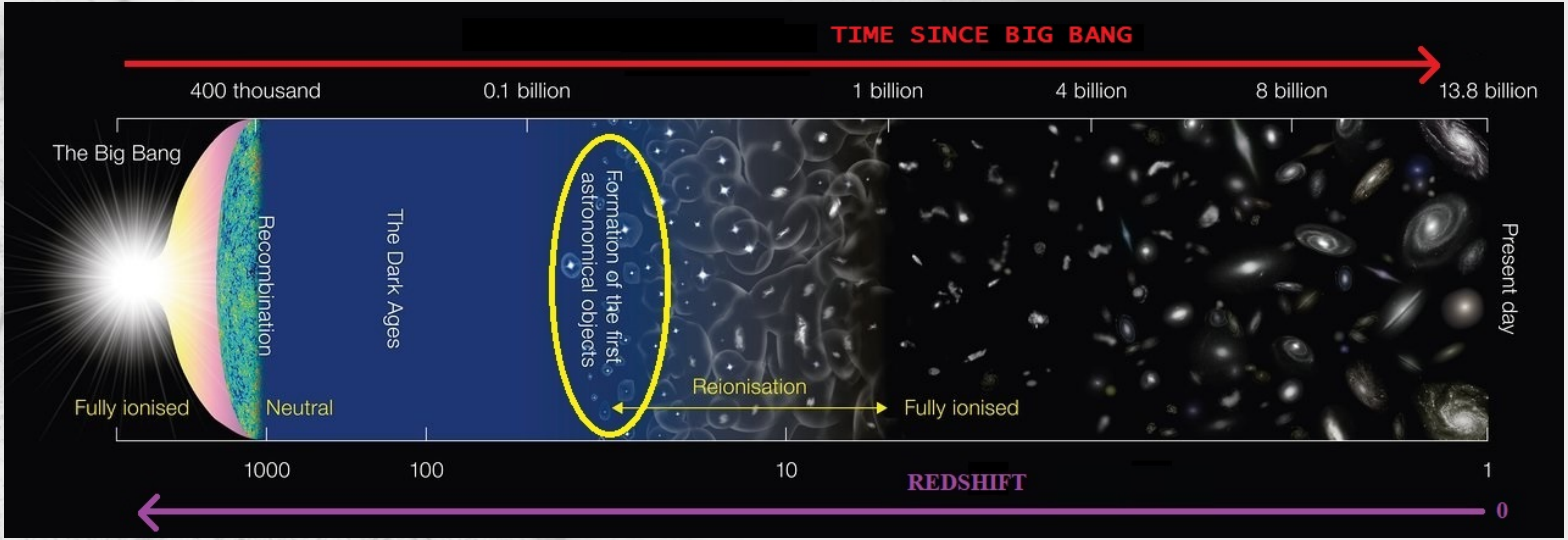

Credits: ESO

THE HIGH REDSHIFT UNIVERSE

The identification and characterization of galaxies at the highest redshifts remains one of the central goals in contemporary astrophysics

Credits: NASA

Prime goals of many legacy surveys

-Hubble Space Telescope (HST)
-James Webb Space Telescope (JWST)

Credits: NASA

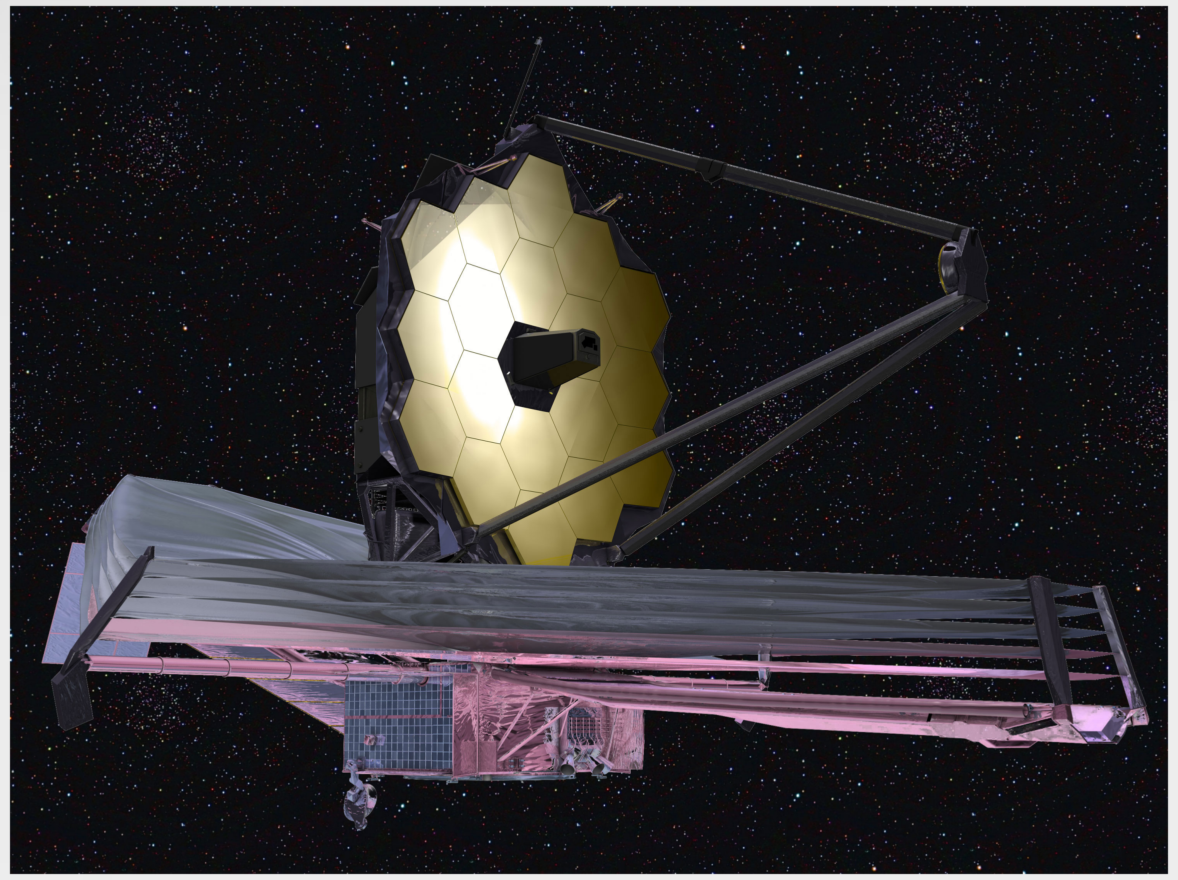

Credits: NASA

REALLY CHALLENGING!!!

SEXTEN CENTER FOR ASTROPHYSICS RICCARDO GIACCONI

The identification and characterization of galaxies at the highest redshifts remains one of the central goals in contemporary astrophysics

Credits: NASA

EXTREME LUMINOSITY DISTANCE

↓

The majority of individual galaxies **INVISIBLE** to ground-based observatories, to HST, and possibly even to JWST.

↓

The **FAINTNESS** of these galaxies limits the available diagnostics

The identification and characterization of galaxies at the highest redshifts remains one of the central goals in contemporary astrophysics

Credits: NASA

RESULTS

-Many galaxy are limited to photometric observations

-Individual far-UV emission lines such as Lyman-α (Small number of cases)

—> Few constraints on the chemical or dynamical properties of the galaxies

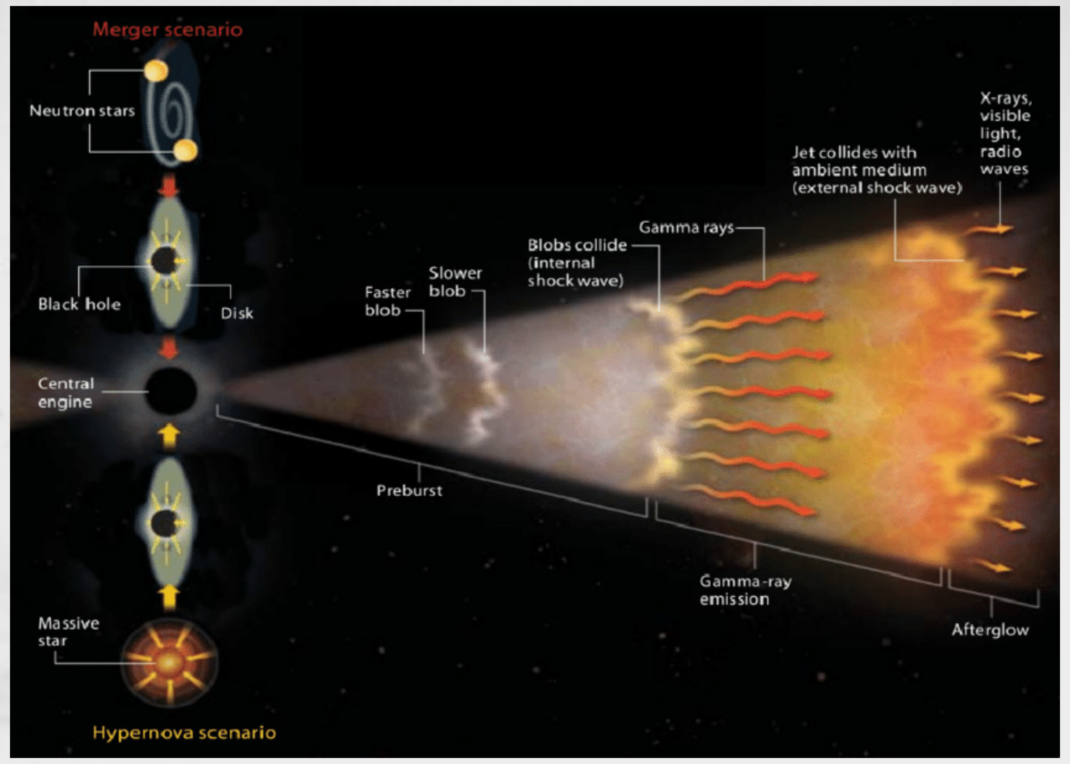

Credits: NASA

GRBs ARE IDEAL TOOLS TO TACKLE THESE ISSUES

See S.D. Vergani's Talk

LGRBs afterglows are unique powerful background sources to probe first galaxies

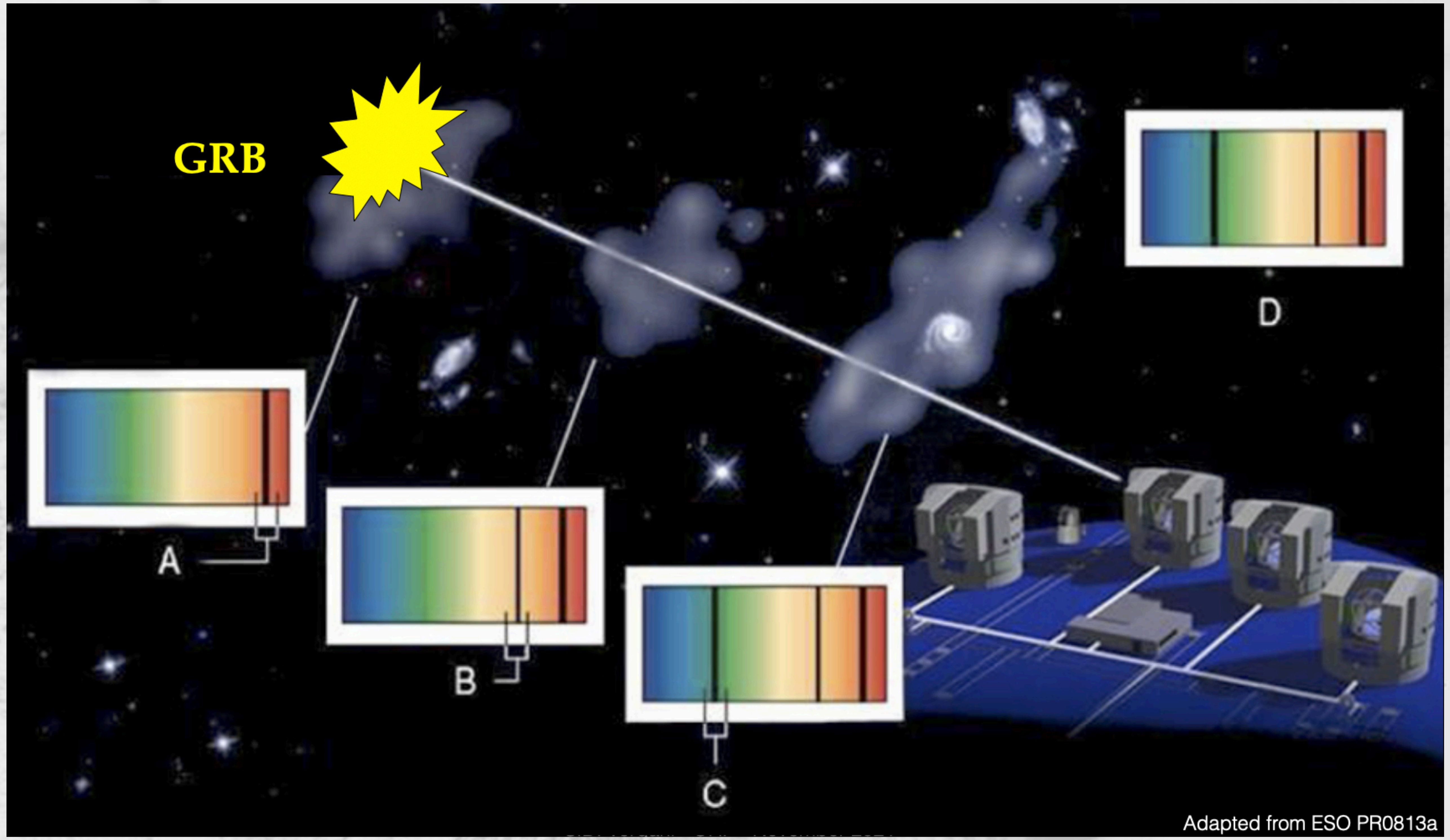

Credits: ESO

-Extremely bright at all redshift

-Associated with the collapse of massive star

-Trace star formation to the highest redshift

-Afterglow emission fades —> Study of LGRB host

-Gas in the ISM (absorption lines Afterglow spectra)

+

Ionised gas (emission lines host galaxy spectra)

ABSORPTION LINES IN HIGH REDSHIFT GRBs SPECTRA

Sexten Center for Astrophysics Riccardo Giacconi

LYMAN ALPHA FOREST
INTERGALACTIC MEDIUM (IGM)

GRB 050730 z=3.968

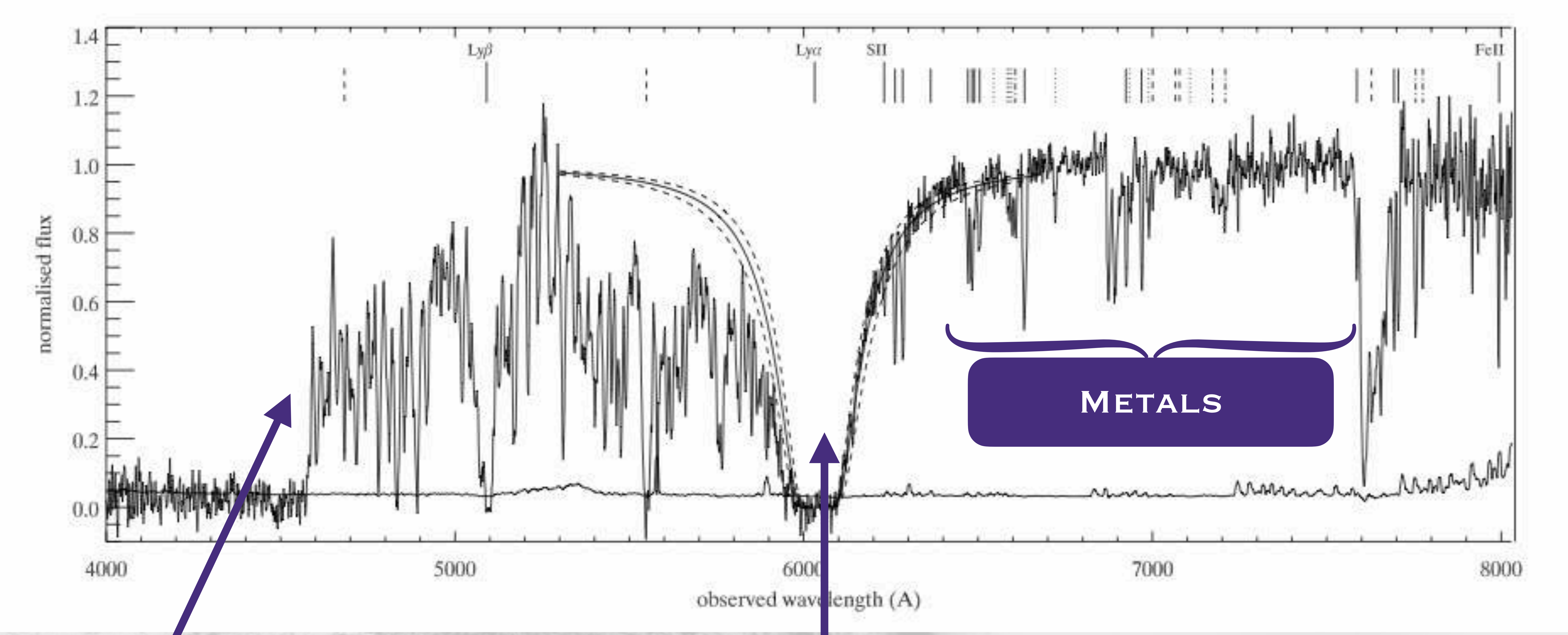

METALS

LYMAN LIMIT

HI (LYMAN ALPHA)
NEUTRAL HYDROGEN

R. L. C. Starling+2005

From the analysis of the absorption lines we can measure:

- ➡ *Redshift of the absorbers*
- ➡ *Column densities of the ions of different chemical elements*

GRB 210905A HOST GALAXY z ~ 6.3

SEXTEN CENTER FOR ASTROPHYSICS RICCARDO GIACCONI

X-Shooter Spectrum

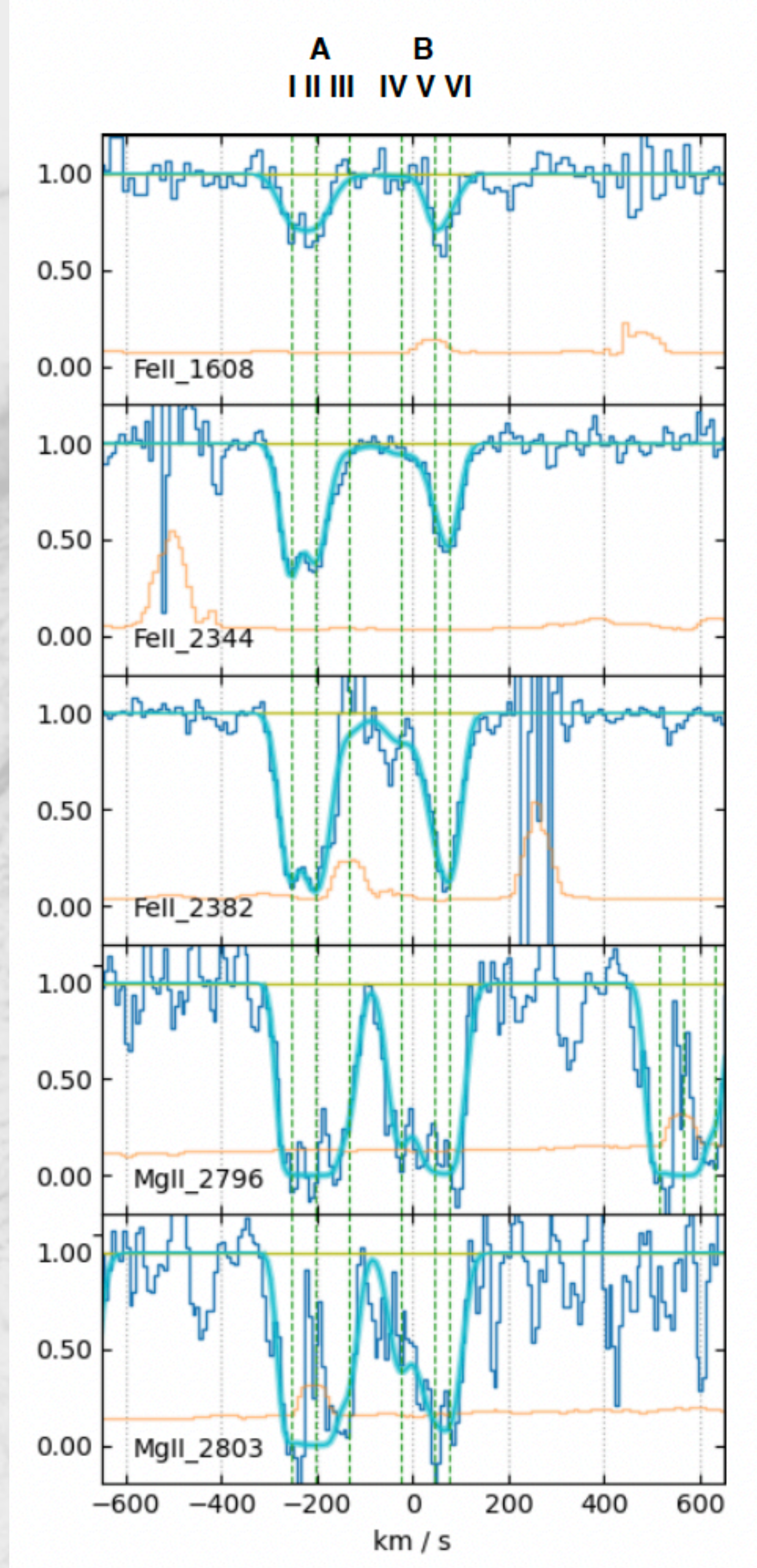

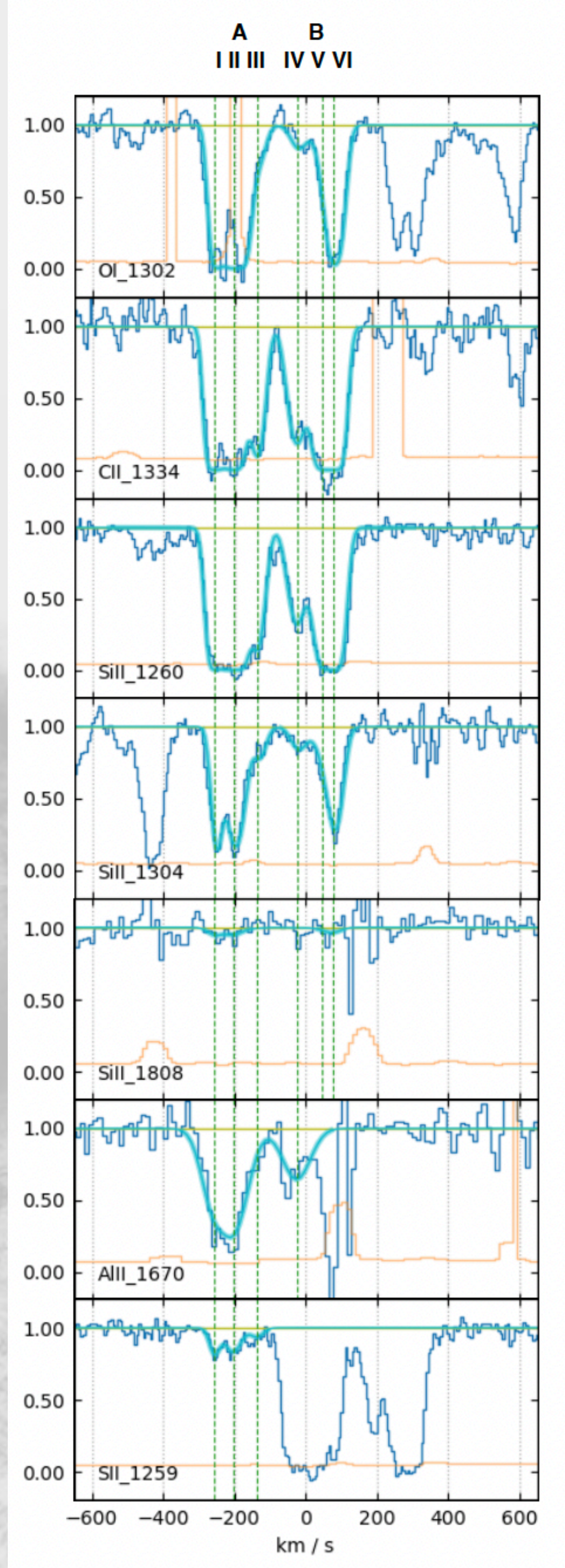

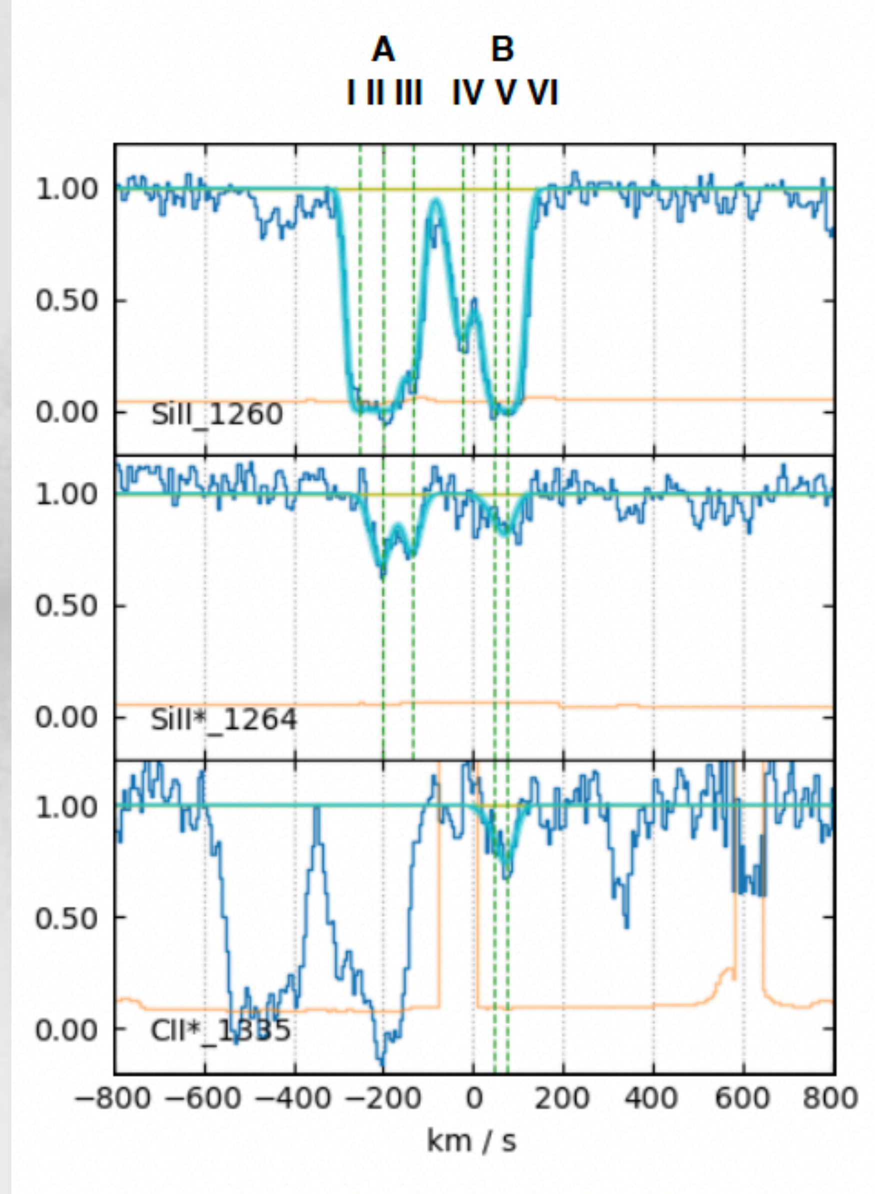

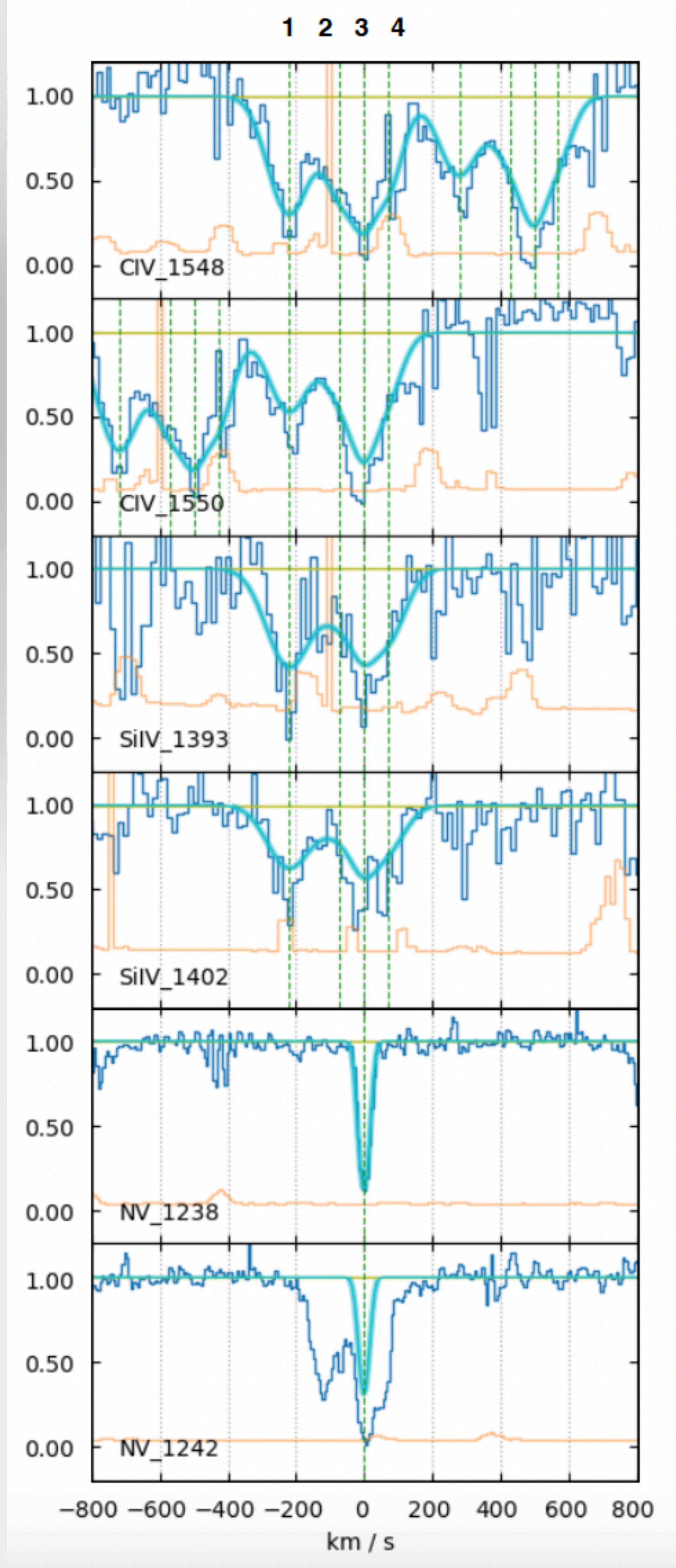

A. Saccardi, S.D. Vergani, A. De Cia et al. 2023 in press

GRB 210905A HOST GALAXY z ~ 6.3

A. Saccardi, S.D. Vergani, A. De Cia et al. 2023 in press

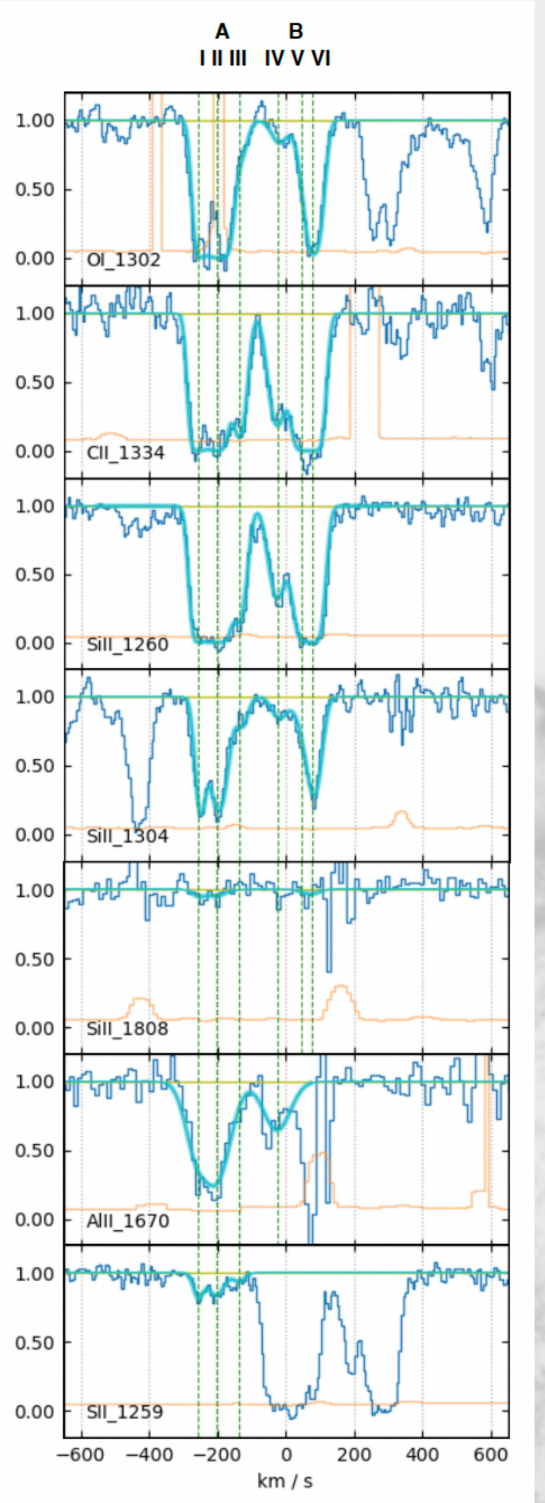

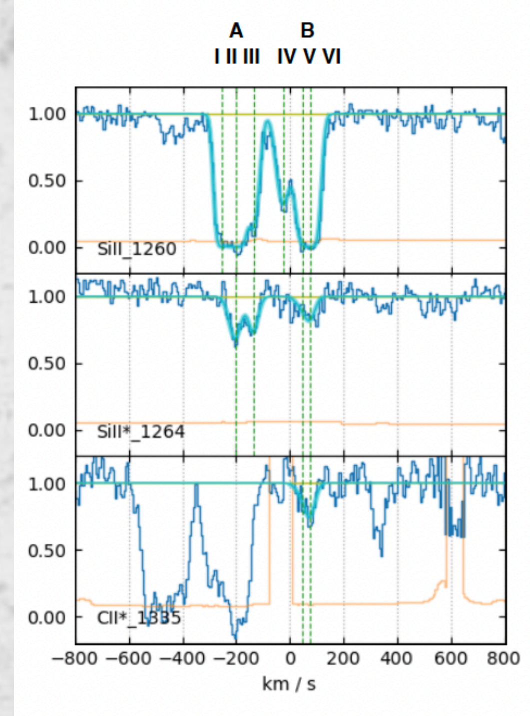

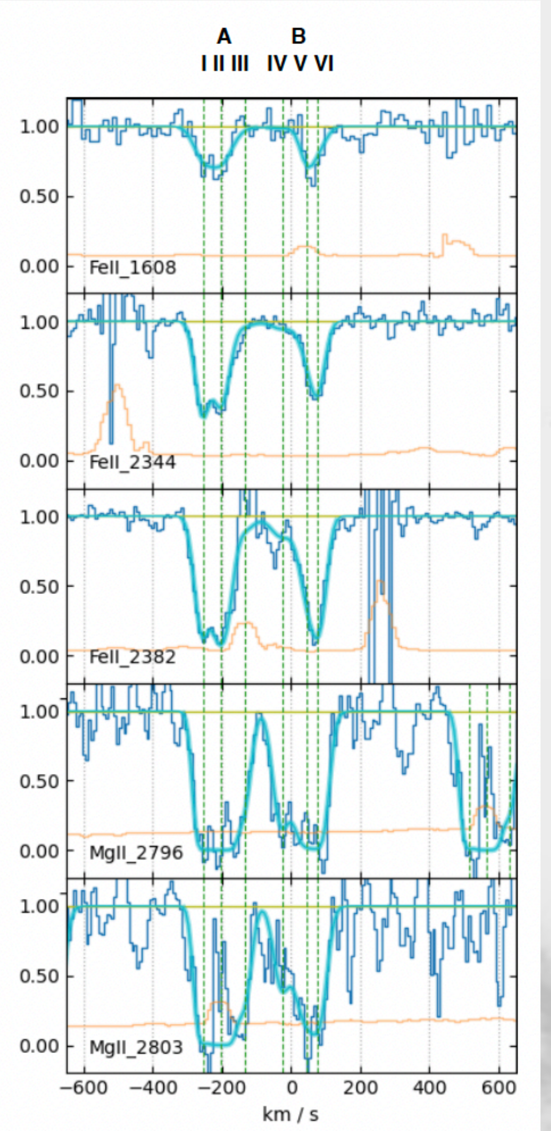

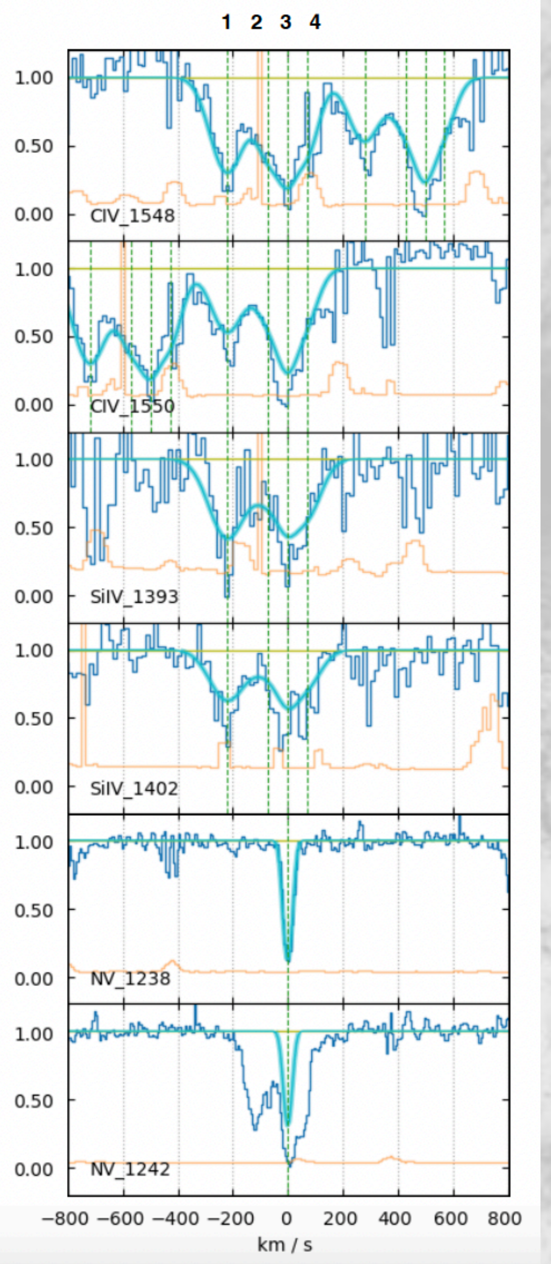

VLT/X-shooter spectrum

- ✴ After ~ 2.53 hours (observer frame)
- ✴ 4 exposures of 1200s (UVB,VIS,NIR)
- ✴ Wavelength range 3 000 - 21 000 Å

Data analysis :

We identify several absorbing systems:

-The highest redshift one is at z=6.312: the host galaxy of GRB 210905A

-Very strong foreground system at z=2.829 (MgII,FeII)

and another at z=5.739 (CII, FeII, CIV, SiIV)

The z = 6.3 system:

-The z~6.3 complex spans ~360 km s^{-1} and is composed of two major systems (A and B) separated by ~300 km s^{-1}, and formed by six components

-Fine-structure lines in both systems (components II, III, V, VI)

GRB 210905A HOST GALAXY z ~ 6.3

SEXTEN CENTER FOR ASTROPHYSICS RICCARDO GIACCONI

A. Saccardi, S.D. Vergani, A. De Cia et al. 2023 in press

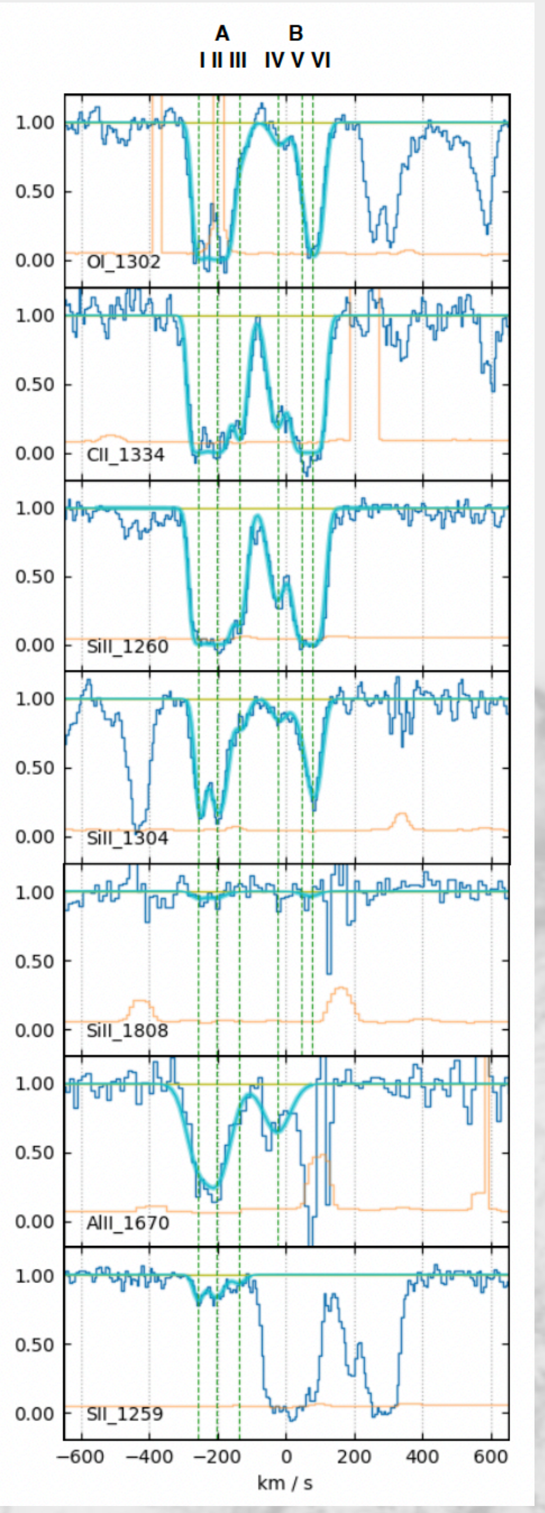

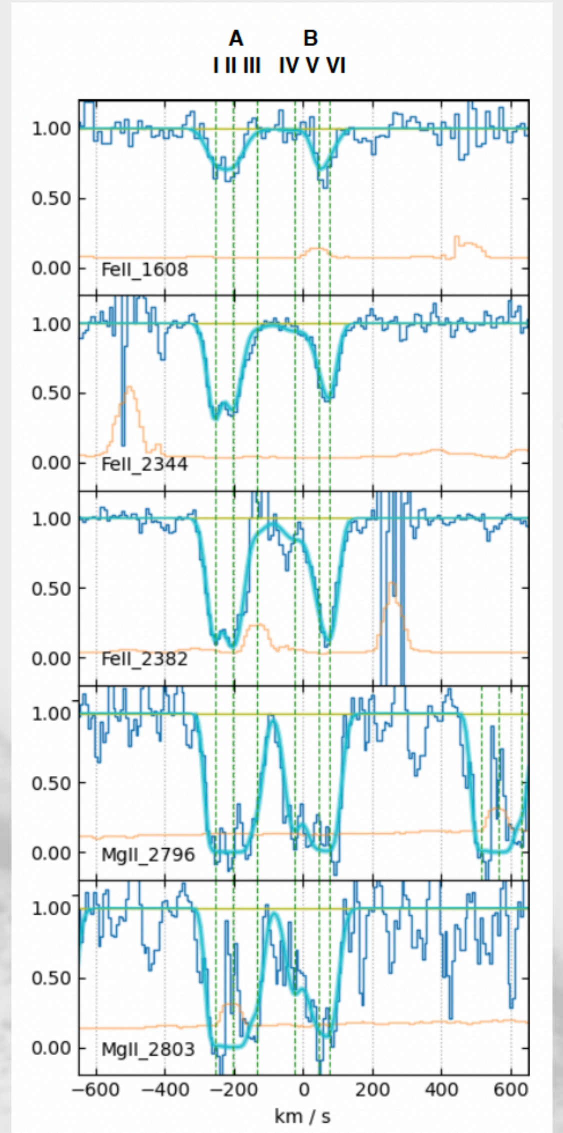

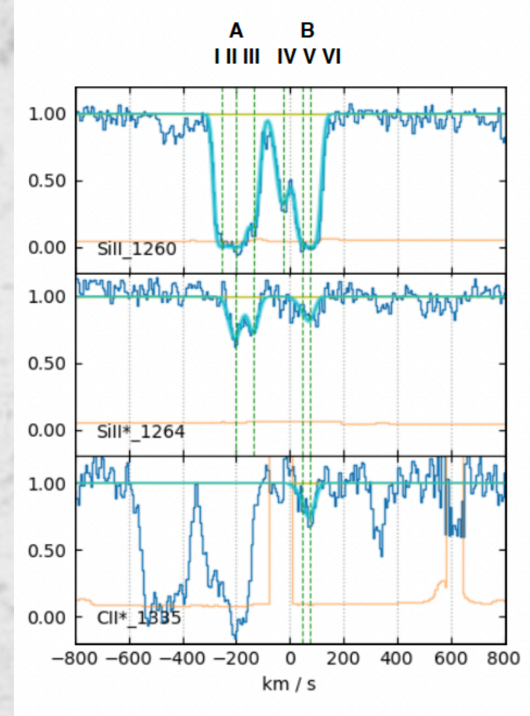

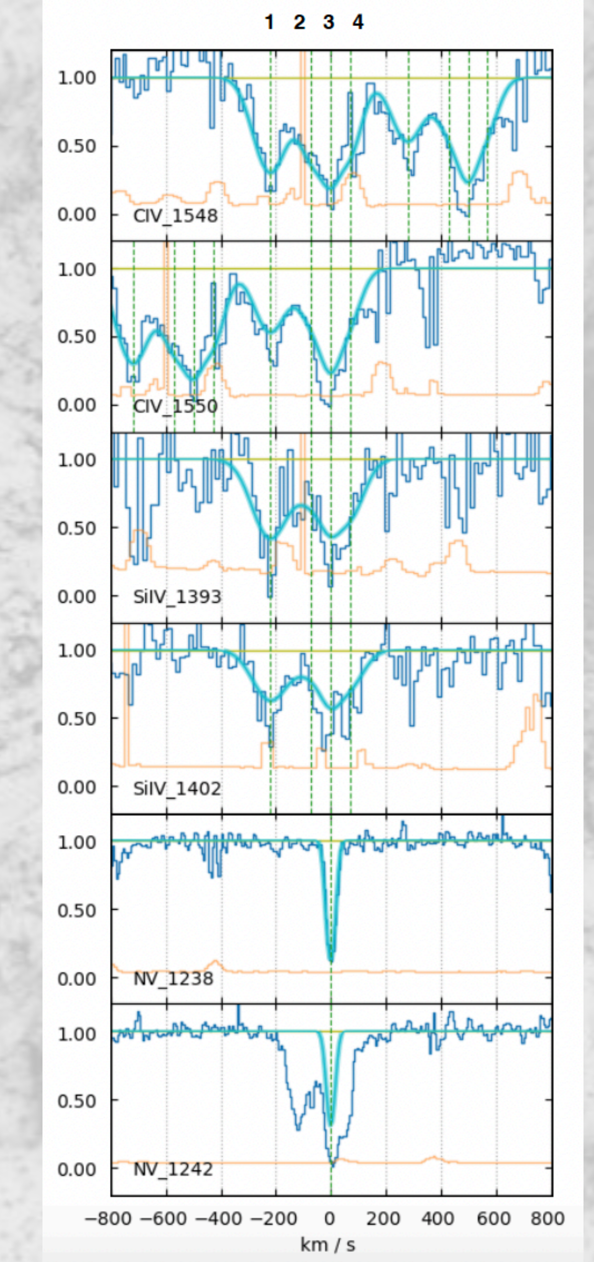

VLT/X-shooter spectrum

- ✳ After ~ 2.53 hours (observer frame)
- ✳ 4 exposures of 1200s (UVB,VIS,NIR)
- ✳ Wavelength range 3 000 - 21 000 Å

From the absorption properties :

- ➡*Metallicity and dust depletion*
- ➡*The distance of the corresponding gas clouds*
  (From the fine structure lines e.g. Vreeswijk+2007; D'Elia+2009)
- ➡*Kinematic of the gas*
- ➡*Chemical abundance pattern*

SEXTEN CENTER FOR ASTROPHYSICS RICCARDO GIACCONI

We perform a detailed analysis of metallicity, chemical enrichment and dust depletion

Abundance patterns: ISM metallicities

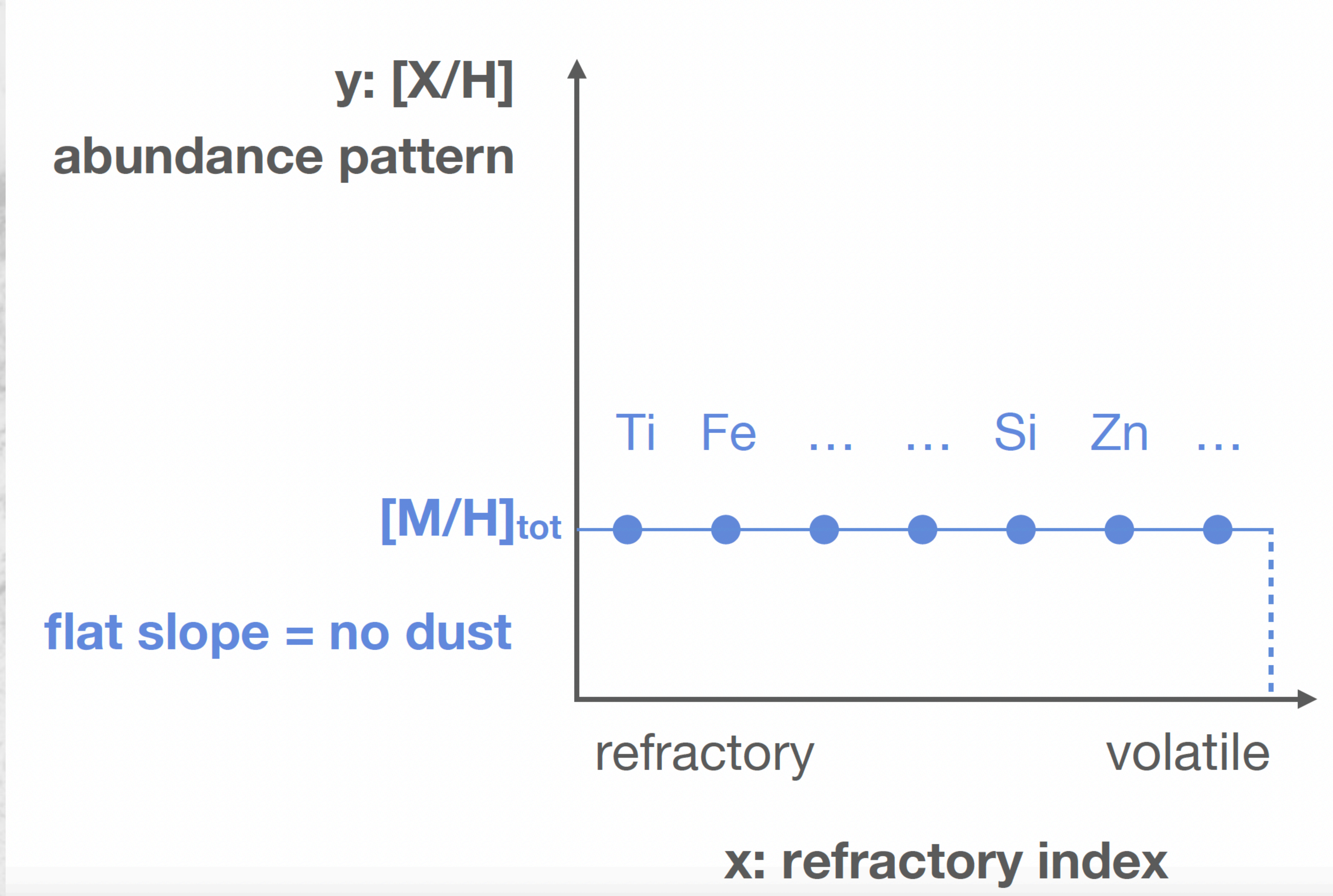

Courtesy of A. De Cia

Following De Cia et al. 2016, De Cia et al. 2021

AXIS

X = How refractory is an element

Y = Elements abundances

FIT

Slope —> $[Zn/Fe]_{fit}$

Intercept —> $[M/H]_{tot}$

GRB 210905A HOST GALAXY z ~ 6.3

We perform a detailed analysis of metallicity, chemical enrichment and dust depletion

Abundance patterns: ISM metallicities + Dust

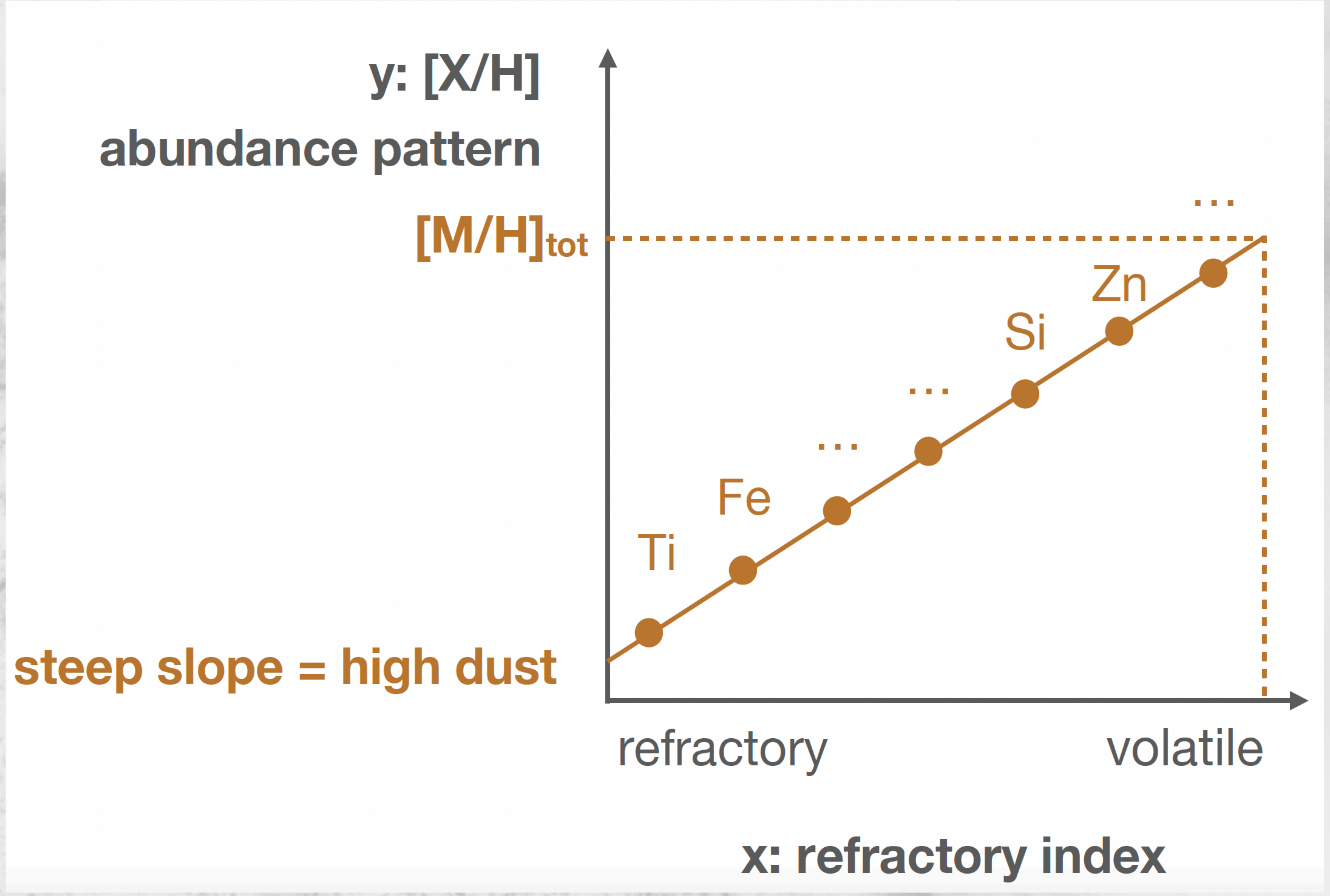

Courtesy of A. De Cia

<u>Following De Cia et al. 2016, De Cia et al. 2021</u>

AXIS

X = How refractory is an element

Y = Elements abundances

FIT

Slope —> $[Zn/Fe]_{fit}$

Intercept —> $[M/H]_{tot}$

GRB 210905A HOST GALAXY z ~ 6.3

SEXTEN CENTER FOR ASTROPHYSICS RICCARDO GIACCONI

We perform a detailed analysis of metallicity, chemical enrichment and dust depletion

Abundance patterns: ISM metallicities + Dust + α-element enhancements

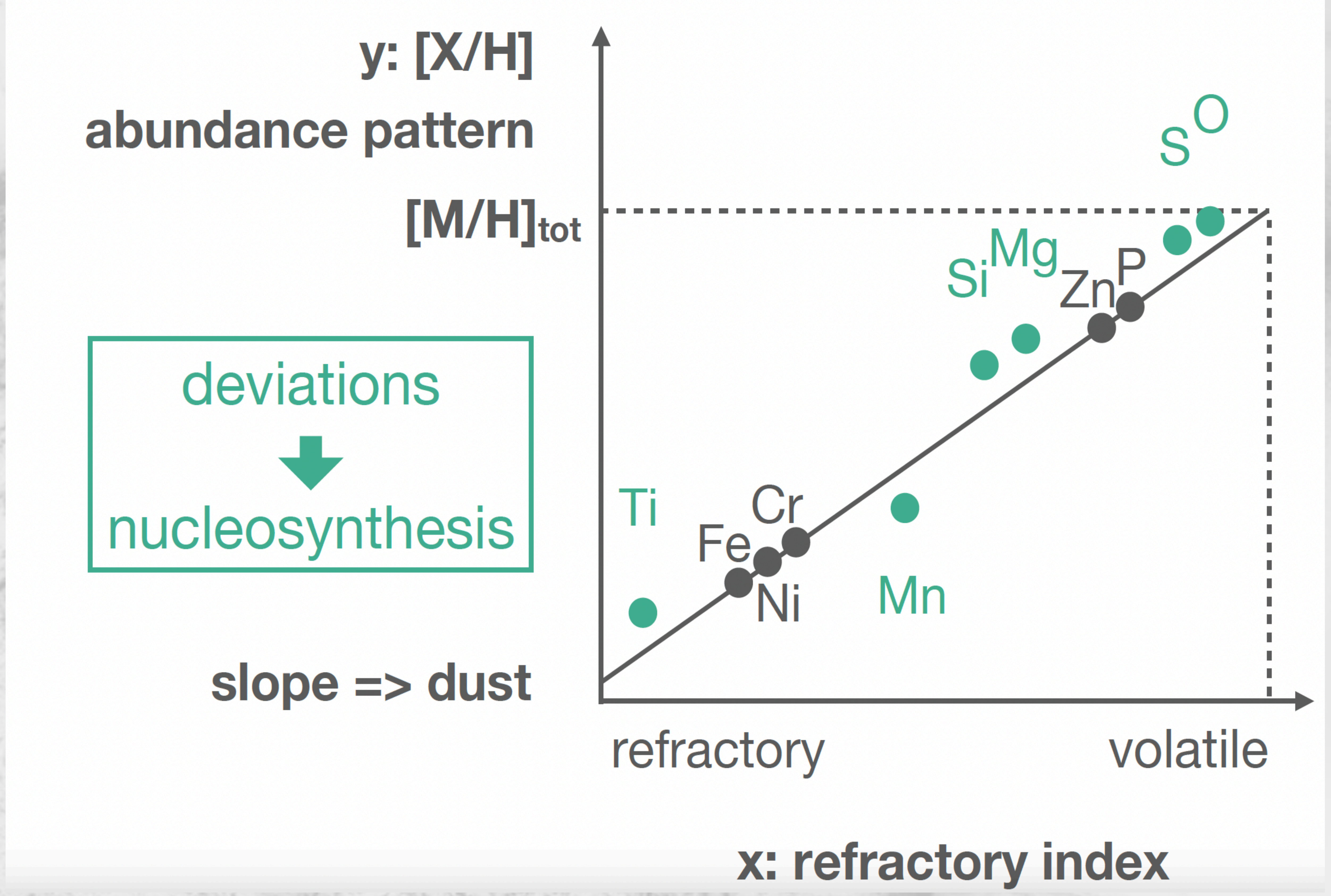

Courtesy of A. De Cia

Following De Cia et al. 2016, De Cia et al. 2021

AXIS

X = How refractory is an element

Y = Elements abundances

FIT

Slope —> $[Zn/Fe]_{fit}$

Intercept —> $[M/H]_{tot}$

We perform a detailed analysis of metallicity, chemical enrichment and dust depletion

The overall host galaxy

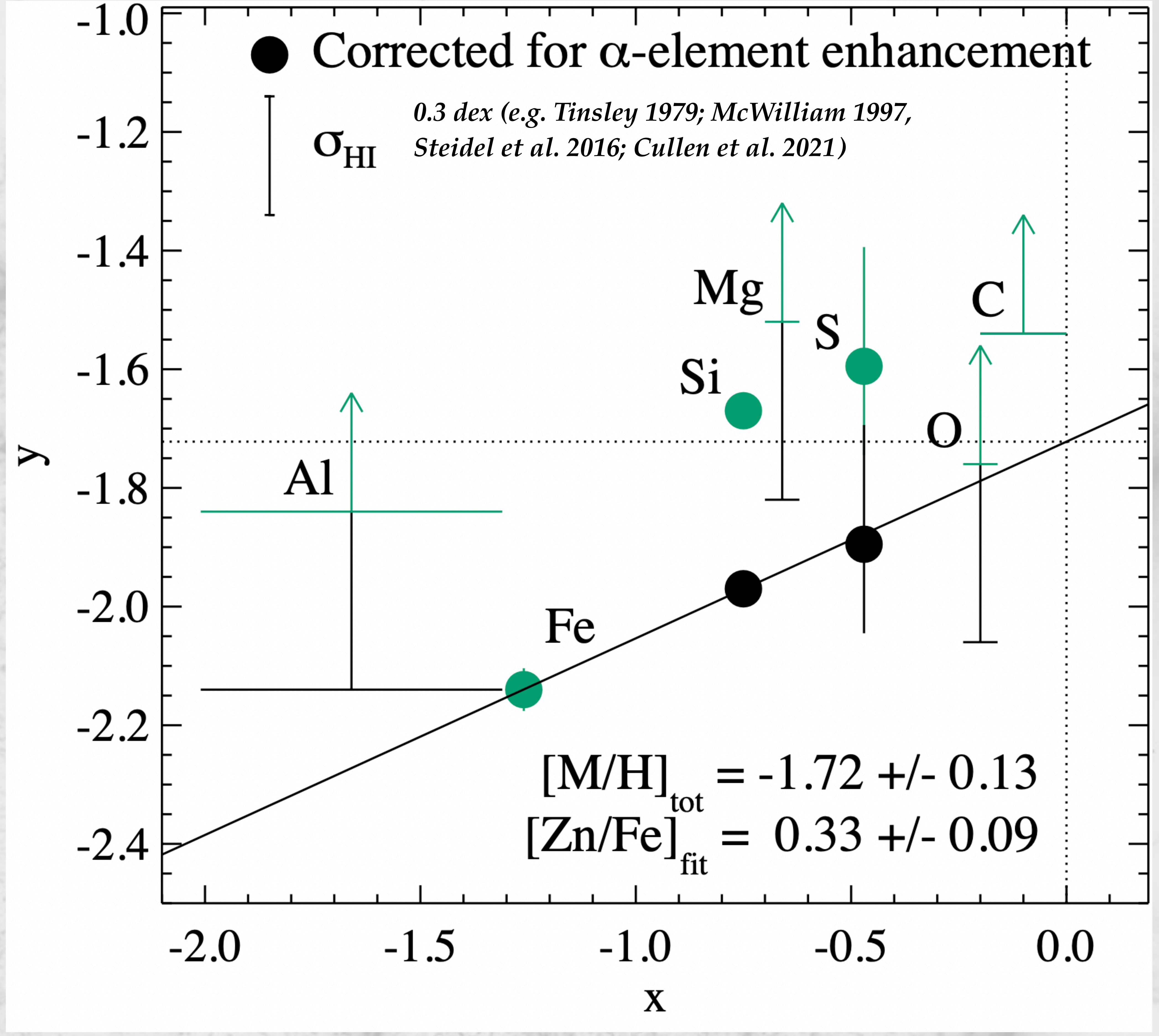

A. Saccardi, S.D. Vergani, A. De Cia et al. 2023 in press

<u>Following De Cia et al. 2016, De Cia et al. 2021</u>

AXIS

X = How refractory is an element

Y = Elements abundances

FIT

Slope —> $[Zn/Fe]_{fit}$

Intercept —> $[M/H]_{tot}$

GRB 210905A HOST GALAXY z ~ 6.3

We perform a detailed analysis of metallicity, chemical enrichment and dust depletion

The overall host galaxy

Component-by-component

A. Saccardi, S.D. Vergani, A. De Cia et al. 2023 in press

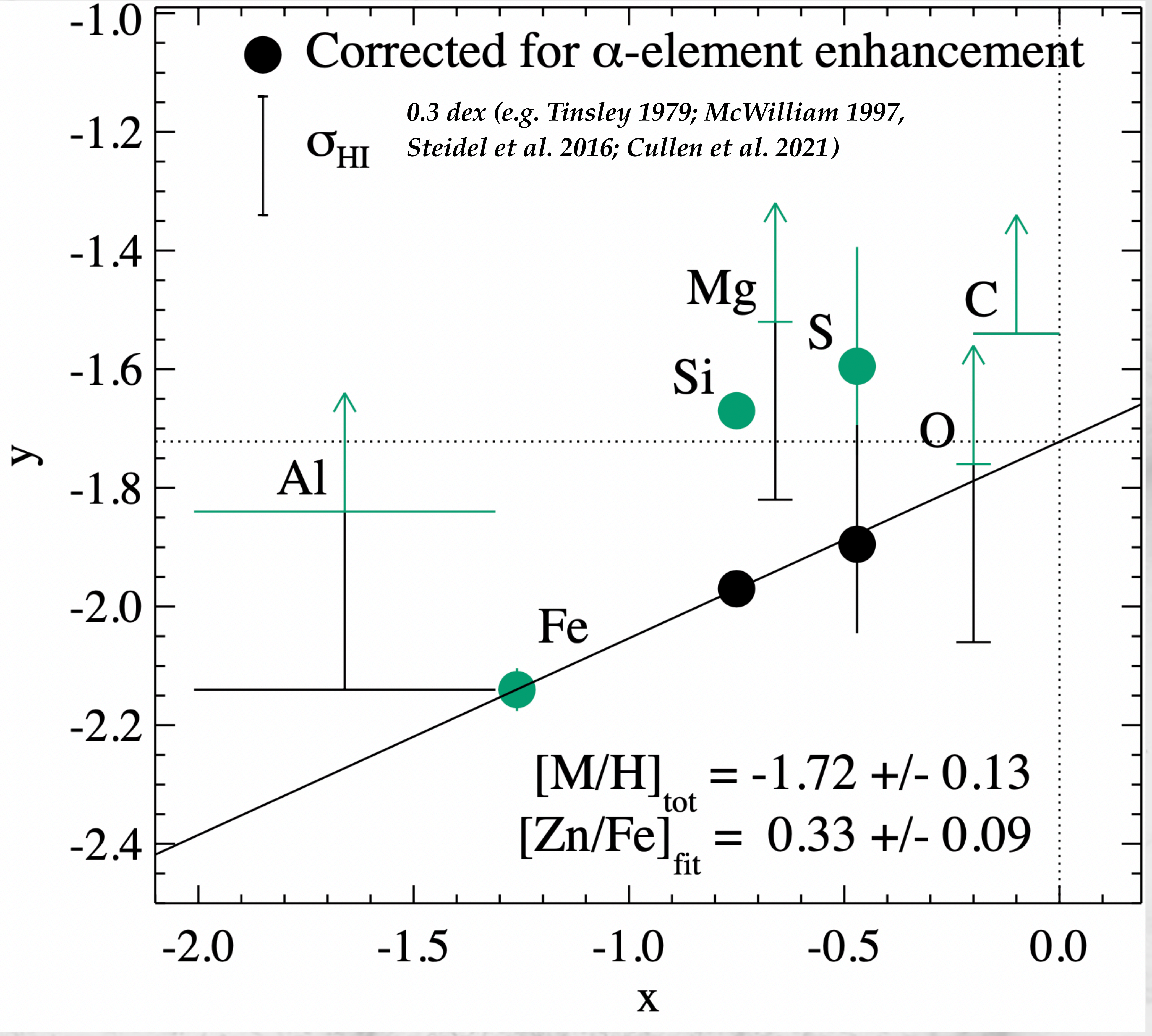

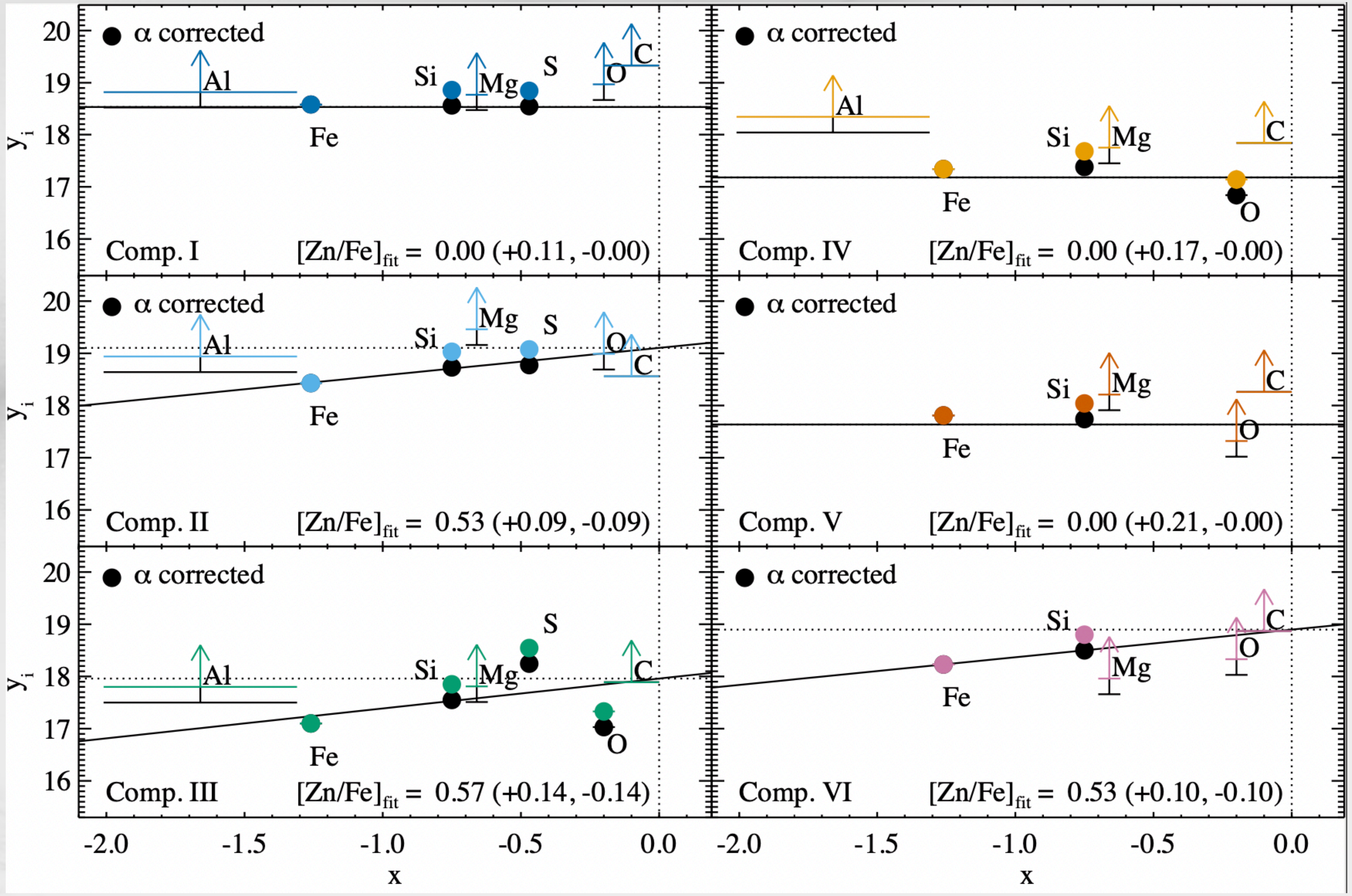

SEXTEN CENTER FOR ASTROPHYSICS RICCARDO GIACCONI

RESULTS

-We find that the dust-corrected metallicity of the GRB host is [M/H] = -1.72 +/- 0.13 and DTM = 0.18 +/- 0.03

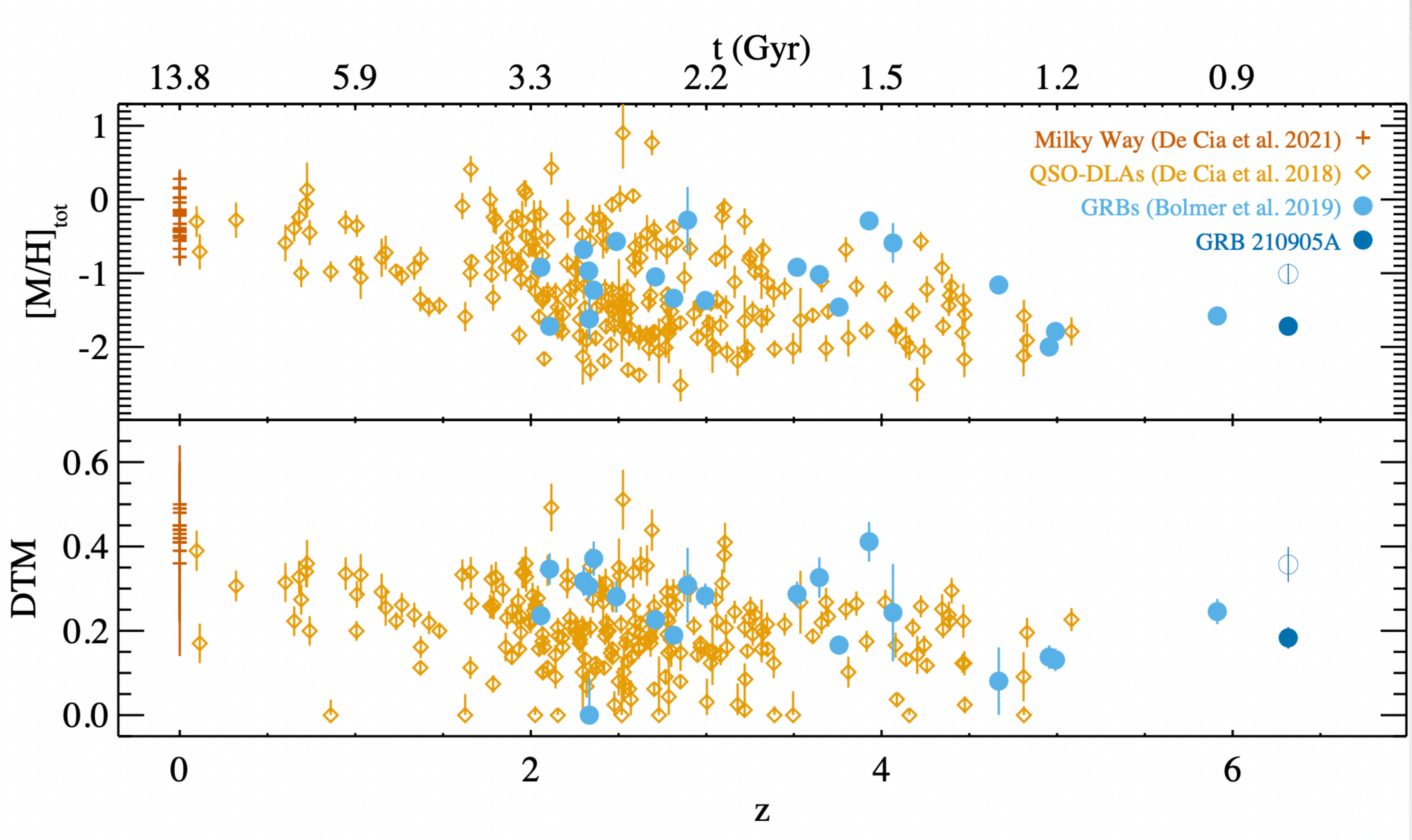

A. Saccardi, S.D. Vergani, A. De Cia et al. 2023 in press

GRB 210905A HOST GALAXY z ~ 6.3

RESULTS

-We find that the dust-corrected metallicity of the GRB host is [M/H] = -1.72 +/- 0.13 and DTM = 0.18 +/- 0.03

-We determine the total abundance pattern and for each component: the deviation from the linear fits, $[X/Fe]_{nucl}$, are due to the effect of nucleosynthesis

A. Saccardi, S.D. Vergani, A. De Cia et al. 2023 in press

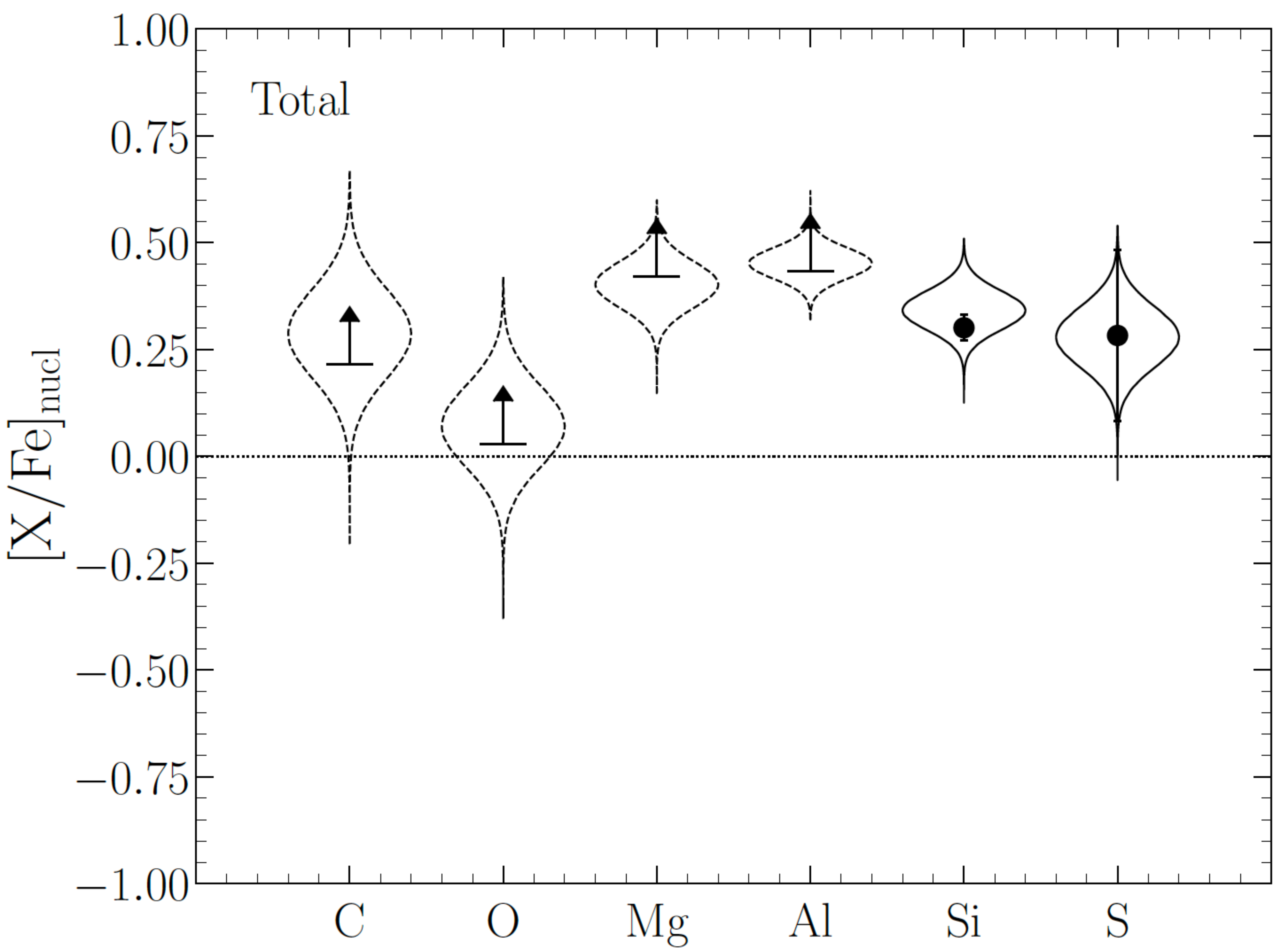

SEXTEN CENTER FOR ASTROPHYSICS RICCARDO GIACCONI

RESULTS

-We find that the dust-corrected metallicity of the GRB host is [M/H] = -1.72 +/- 0.13 and DTM = 0.18 +/- 0.03

-We determine the total abundance pattern and for each component: the deviation from the linear fits, $[X/Fe]_{nucl}$, are due to the effect of nucleosynthesis

A. Saccardi, S.D. Vergani, A. De Cia et al. 2023 in press

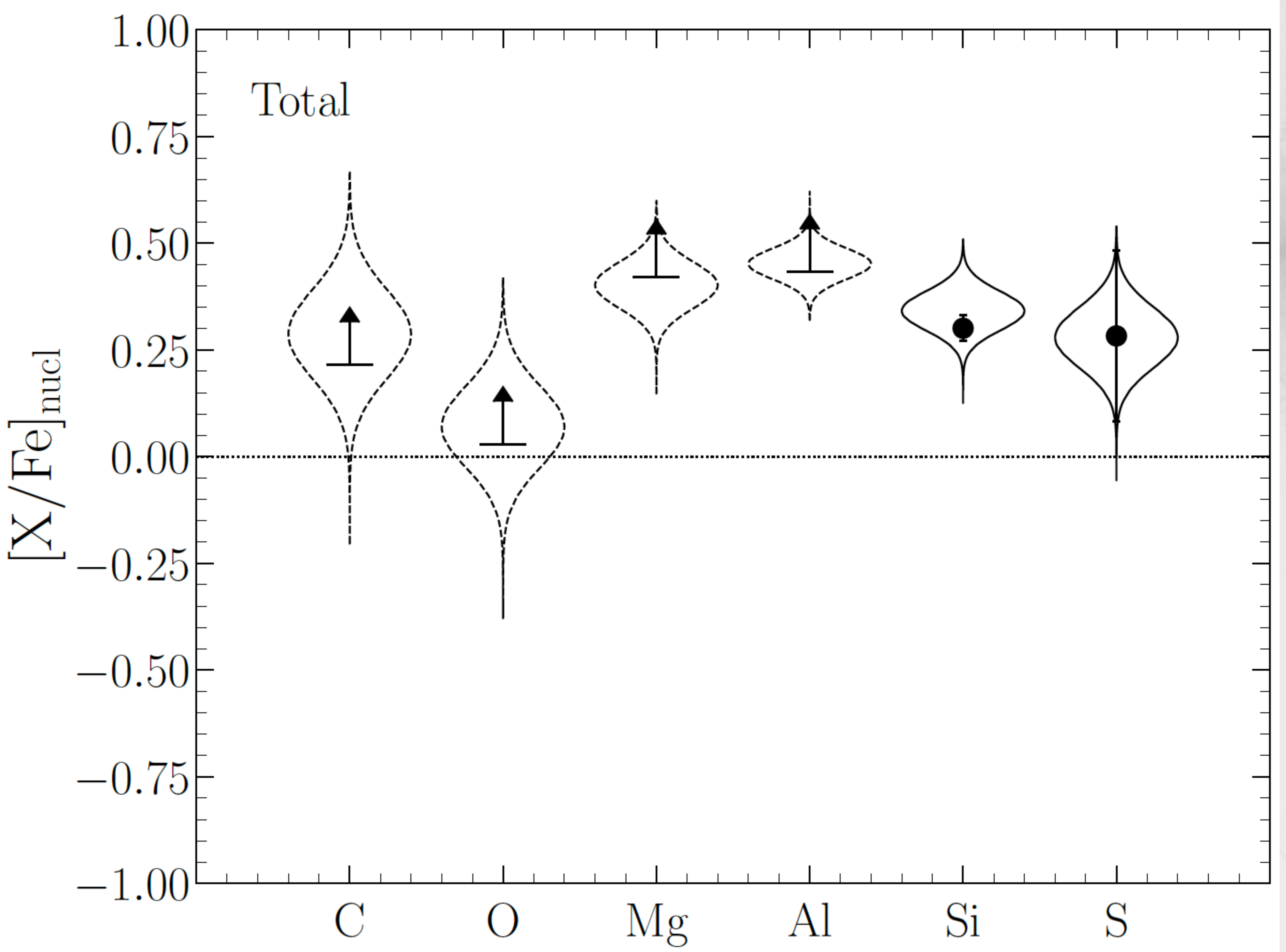

The global observed pattern can be explained by nucleosynthesis due to core-collapse SNe and massive (S-)AGB stars.

(e.g., Masseron et al. 2020)

SEXTEN CENTER FOR ASTROPHYSICS RICCARDO GIACCONI

RESULTS

-We find that the dust-corrected metallicity of the GRB host is [M/H] = -1.72 +/- 0.13 and DTM = 0.18 +/- 0.03

-We determine the total abundance pattern and for each component: the deviation from the linear fits, $[X/Fe]_{nucl}$, are due to the effect of nucleosynthesis

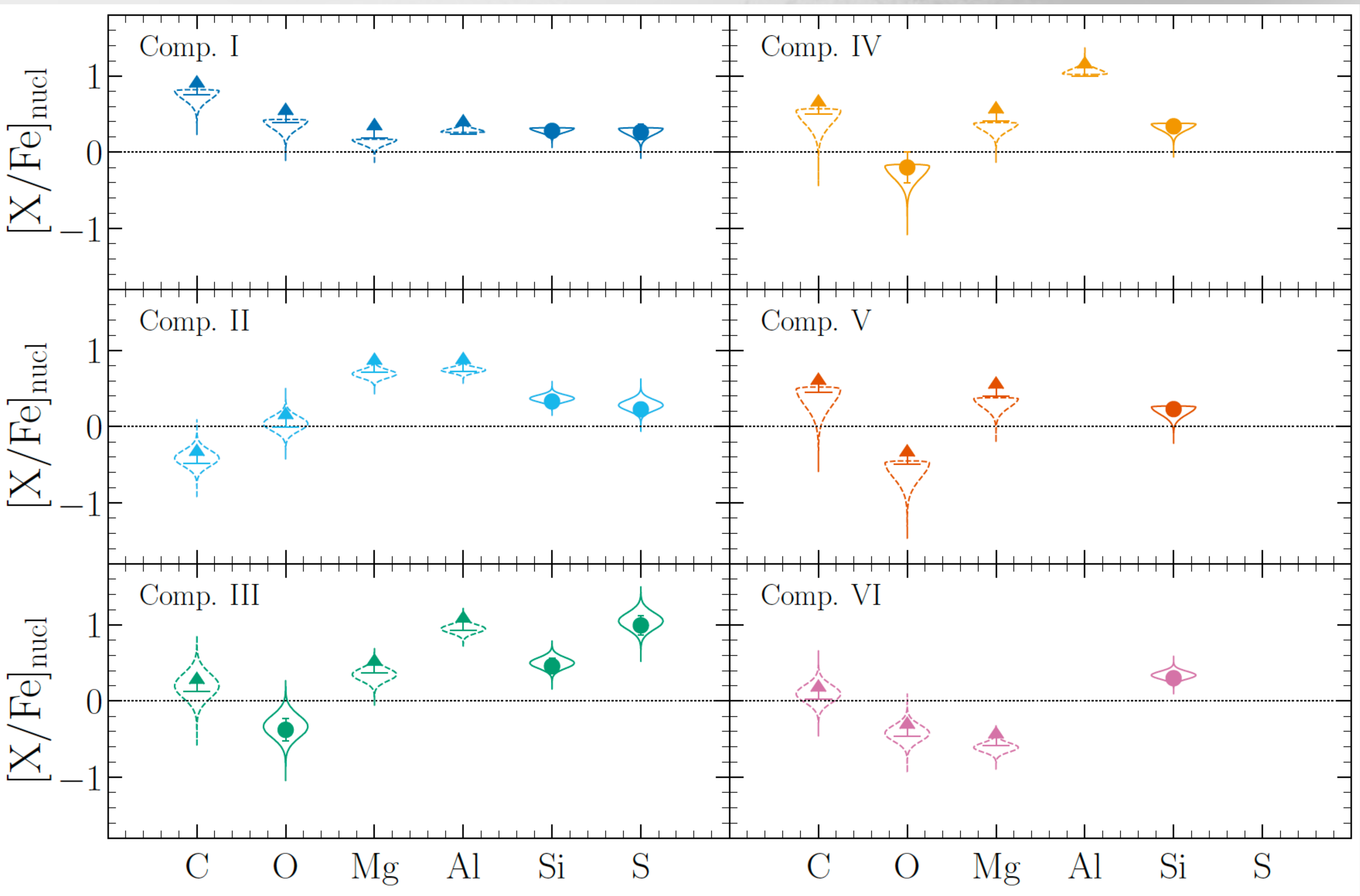

A. Saccardi, S.D. Vergani, A. De Cia et al. 2023 in press

GRB 210905A HOST GALAXY z ~ 6.3

SEXTEN CENTER FOR ASTROPHYSICS RICCARDO GIACCONI

RESULTS

-We find that the dust-corrected metallicity of the GRB host is [M/H] = -1.72 +/- 0.13 and DTM = 0.18 +/- 0.03

-We determine the total abundance pattern and for each component: the deviation from the linear fits, $[X/Fe]_{nucl}$, are due to the effect of nucleosynthesis

A. Saccardi, S.D. Vergani, A. De Cia et al. 2023 in press

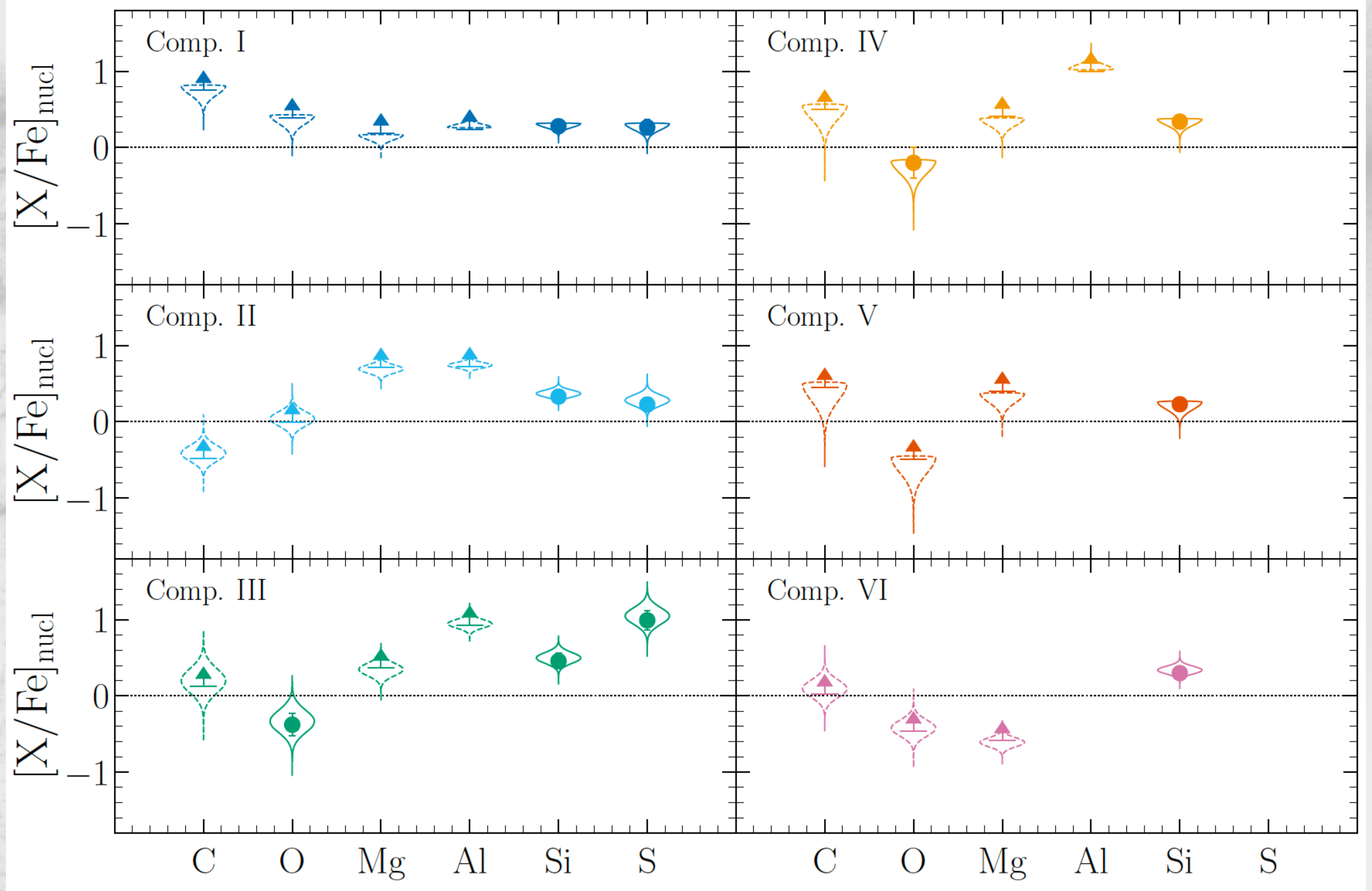

Over-abundance of aluminium
Under-abundance of oxygen:

-typical of some stars found in globular clusters and dwarf galaxies

-the best candidates are massive AGB stars and fast rotating massive stars

(e.g., Prantzos et al. 2007; Fulbright et al. 2007; Alves-Brito et al. 2010)

SEXTEN CENTER FOR ASTROPHYSICS RICCARDO GIACCONI

RESULTS

-We find that the dust-corrected metallicity of the GRB host is [M/H] = -1.72 +/- 0.13 and DTM = 0.18 +/- 0.03

-We determine the total abundance pattern and for each component: the deviation from the linear fits, $[X/Fe]_{nucl}$, are due to the effect of nucleosynthesis

-We calculate the distance of the corresponding gas clouds from the GRB (~7kpc)

UV-Pumping

↓

Excite the absorber atoms and ions to a principal quantum number above the fundamental

↓

By a spontaneous emission, the fine structure lines of the fundamental state are populated

+

Photoionization code

INPUT:
-INCIDENCE FLUX
-INITIAL COLUMN DENSITIES

↓

OUTPUT:
-DISTANCE

GRB 210905A HOST GALAXY z ~ 6.3

SEXTEN CENTER FOR ASTROPHYSICS RICCARDO GIACCONI

RESULTS

-We find that the dust-corrected metallicity of the GRB host is [M/H] = -1.72 +/- 0.13 and DTM = 0.18 +/- 0.03

-We determine the total abundance pattern and for each component: the deviation from the linear fits, $[X/Fe]_{nucl}$, are due to the effect of nucleosynthesis

-We calculate the distance of the corresponding gas clouds from the GRB (~7kpc)

A. Saccardi, S.D. Vergani, A. De Cia et al. 2023 in press

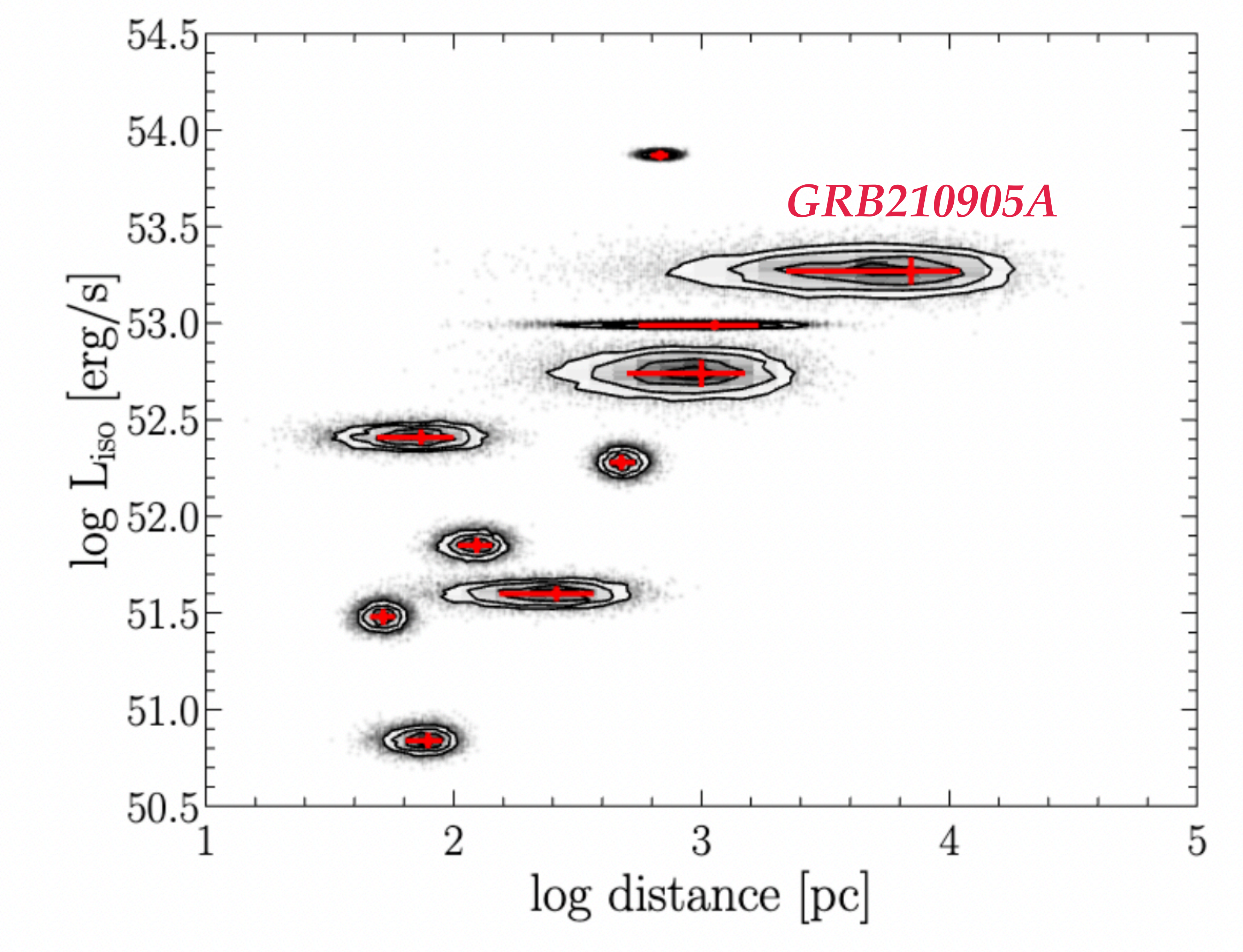

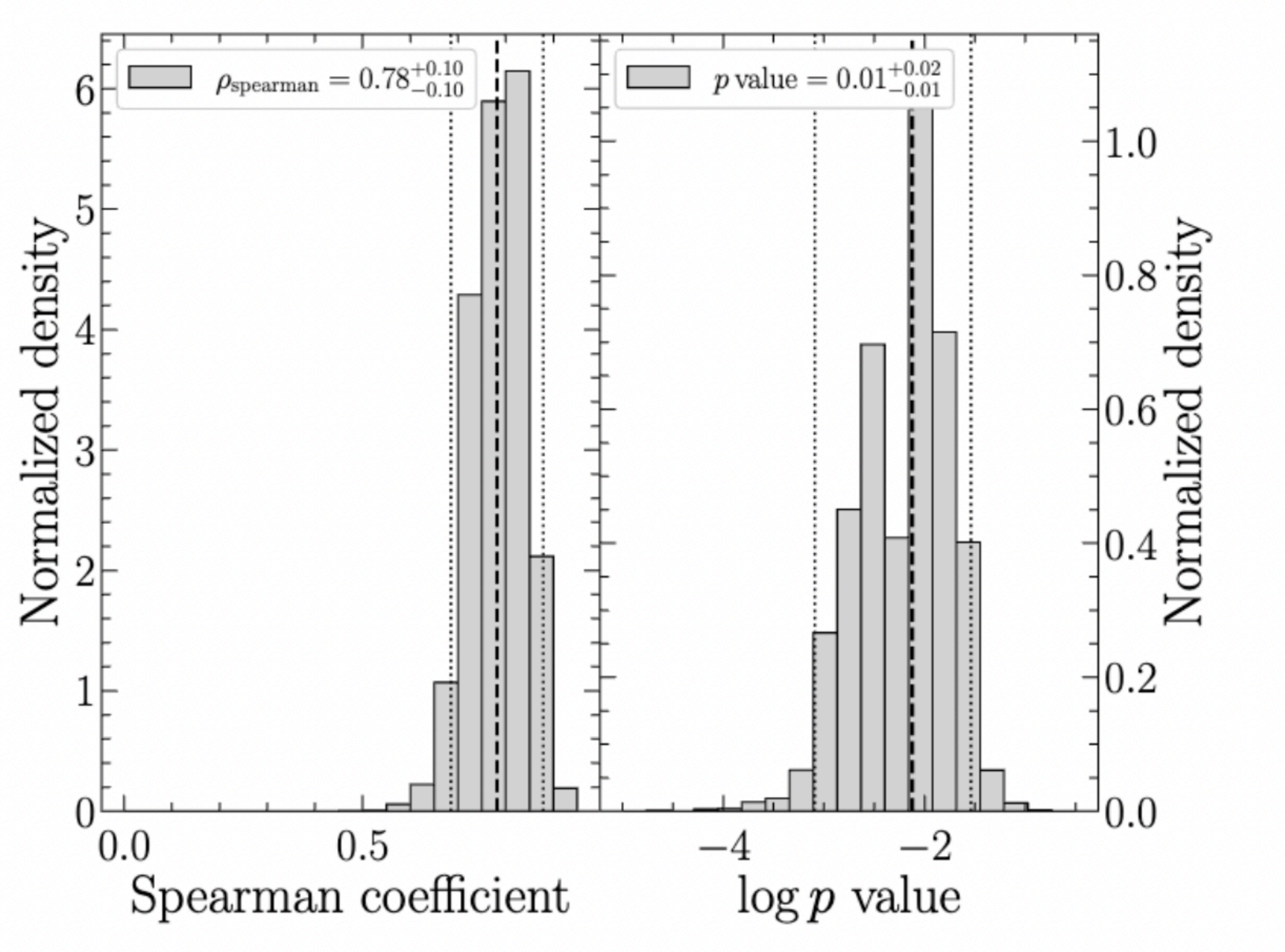

Saccardi et al. 2023 (In press)

GRB210905A

log L_{iso} = 53.27 +/- 0.7 erg s^{-1}

$E_{X,ag}$= 8.8x10^{52} erg

α (temporal slope) = 0.74

β (spectral slope) = 1.13

Krongold & Prochaska 2013

GRB050730

log L_{iso} = 51.85 +/- 0.4 erg s^{-1}

$E_{X,ag}$ = 2.7x10^{51} erg

α (temporal slope) = 1

β (spectral slope) = 1

Using the burst luminosity and the spectral and temporal parameters (Rossi et al. 2022), we determined a number of ionizing photons ~ 30 times higher than the GRB050730 average value

$$\mathcal{N} = \int_{\nu_1}^{\nu_2} N_\nu(\nu,t)\,\mathrm{d}\nu = N_0 \int_{\nu_1}^{\nu_2} \left(\frac{\nu}{\nu_1}\right)^{-2} \mathrm{d}\nu = N_0\nu_1 \int_{1}^{\nu_2/\nu_1} \frac{1}{x^2}\,\mathrm{d}x = N_0\nu_1\left(1-\frac{\nu_1}{\nu_2}\right) =$$
$$= \frac{E\nu_1}{h\nu_1^2 \ln(\nu_2/\nu_1)}\left(1-\frac{\nu_1}{\nu_2}\right) = \frac{E}{h\nu_1}\frac{1}{\ln(\nu_2/\nu_1)}\left(1-\frac{\nu_1}{\nu_2}\right)$$

v1=0.3kev

v2=10kev

t1=100s

t2=10^4a

GRB 210905A HOST GALAXY z ~ 6.3

RESULTS

-We find that the dust-corrected metallicity of the GRB host is [M/H] = -1.72 +/- 0.13 and DTM = 0.18 +/- 0.03

-We determine the total abundance pattern and for each component: the deviation from the linear fits, $[X/Fe]_{nucl}$, are due to the effect of nucleosynthesis

-We calculate the distance of the corresponding gas clouds from the GRB (~7kpc)

-Different scenarios can explain the kinematics of this complex system (galaxy merger/interaction, galaxy group, clumpy structure…)

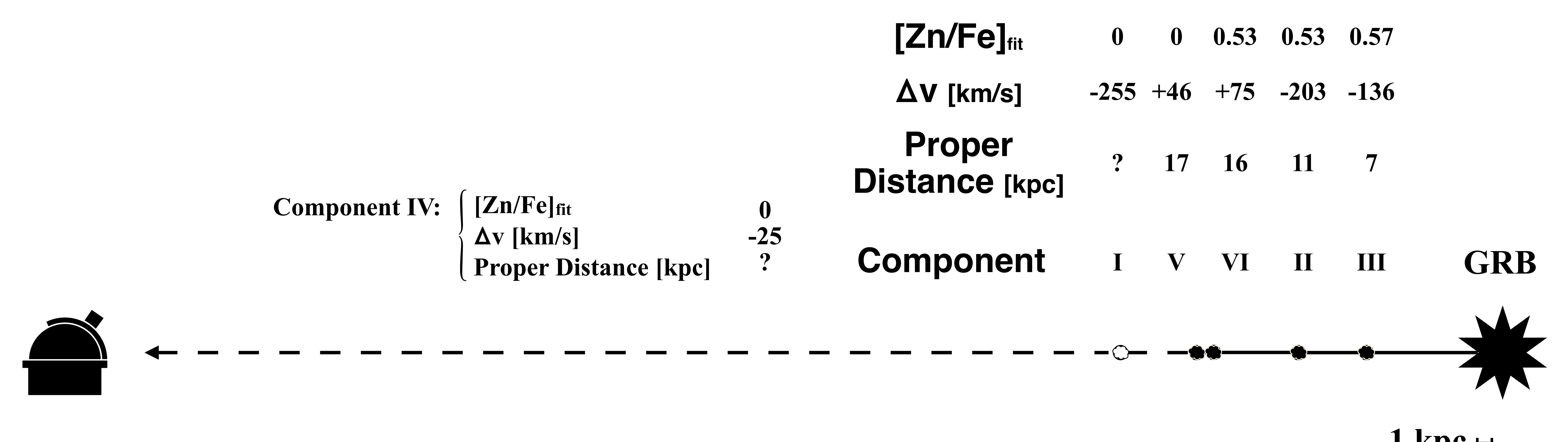

A. Saccardi, S.D. Vergani, A. De Cia et al. 2023 in press

GRB 210905A HOST GALAXY z ~ 6.3

RESULTS

-We find that the dust-corrected metallicity of the GRB host is [M/H] = -1.72 +/- 0.13 and DTM = 0.18 +/- 0.03

-We determine the total abundance pattern and for each component: the deviation from the linear fits, $[X/Fe]_{nucl}$, are due to the effect of nucleosynthesis

-We calculate the distance of the corresponding gas clouds from the GRB (~7kpc)

-Different scenarios can explain the kinematics of this complex system (galaxy merger/interaction, galaxy group, clumpy structure…)

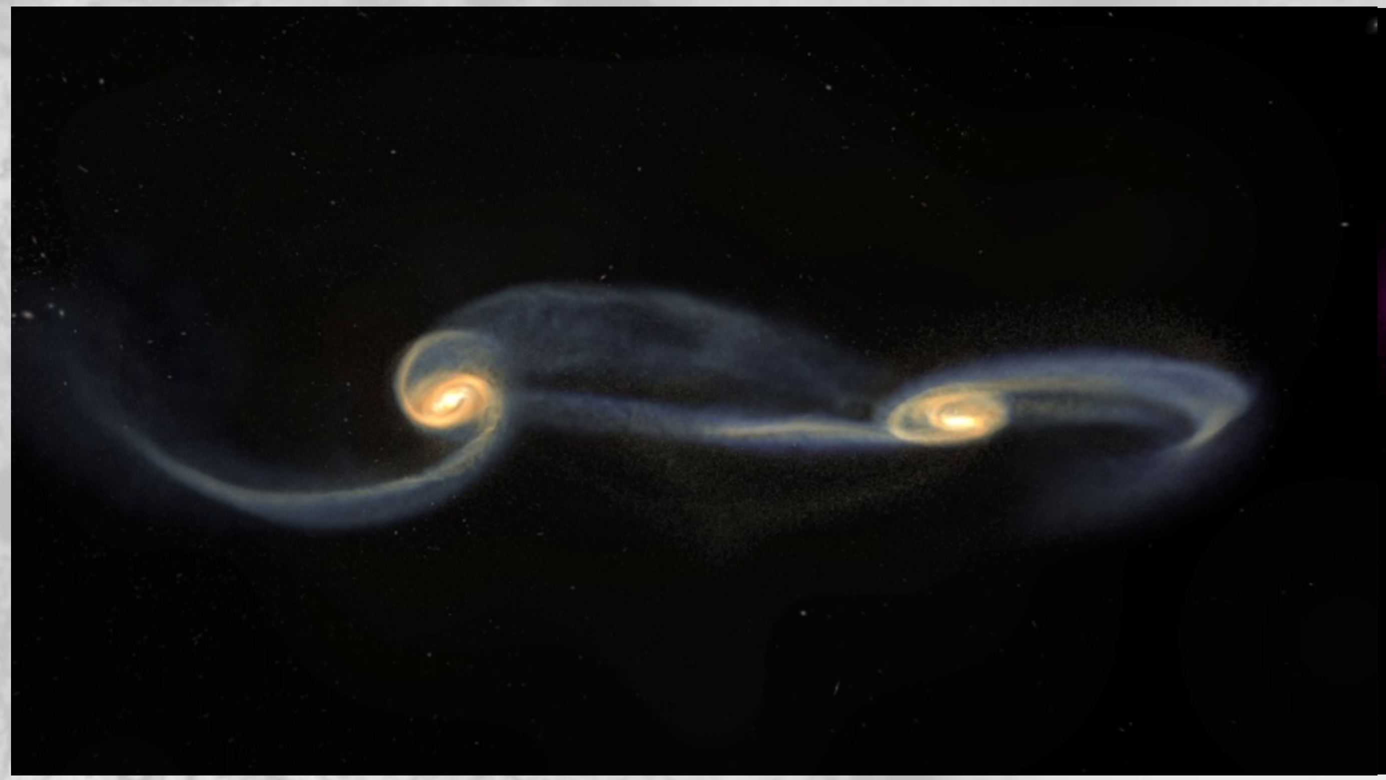

Credits: NASA

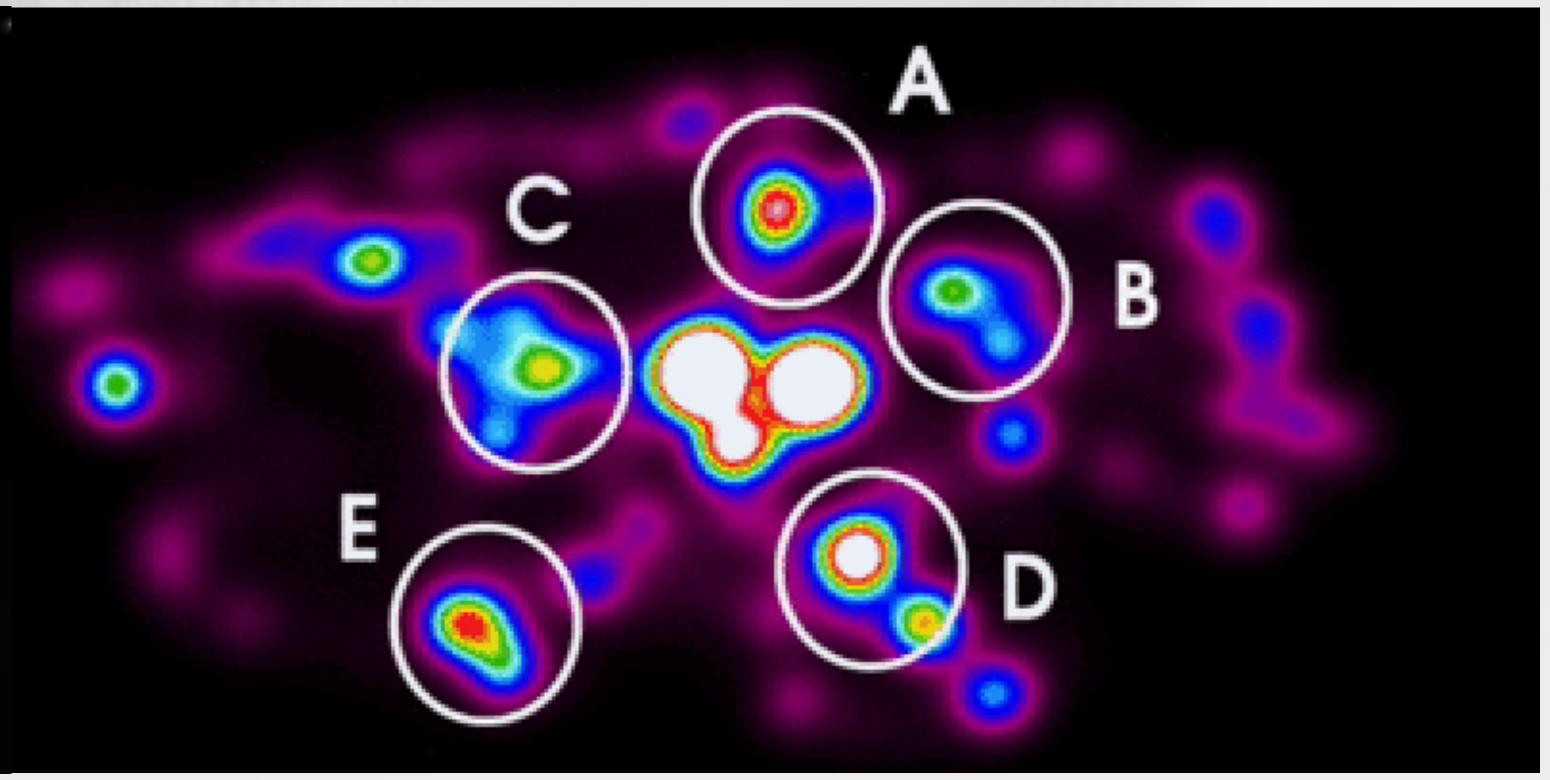

Credits: M. Behrendt - USM

SEXTEN CENTER FOR ASTROPHYSICS RICCARDO GIACCONI

Rest-frame UV spectroscopy

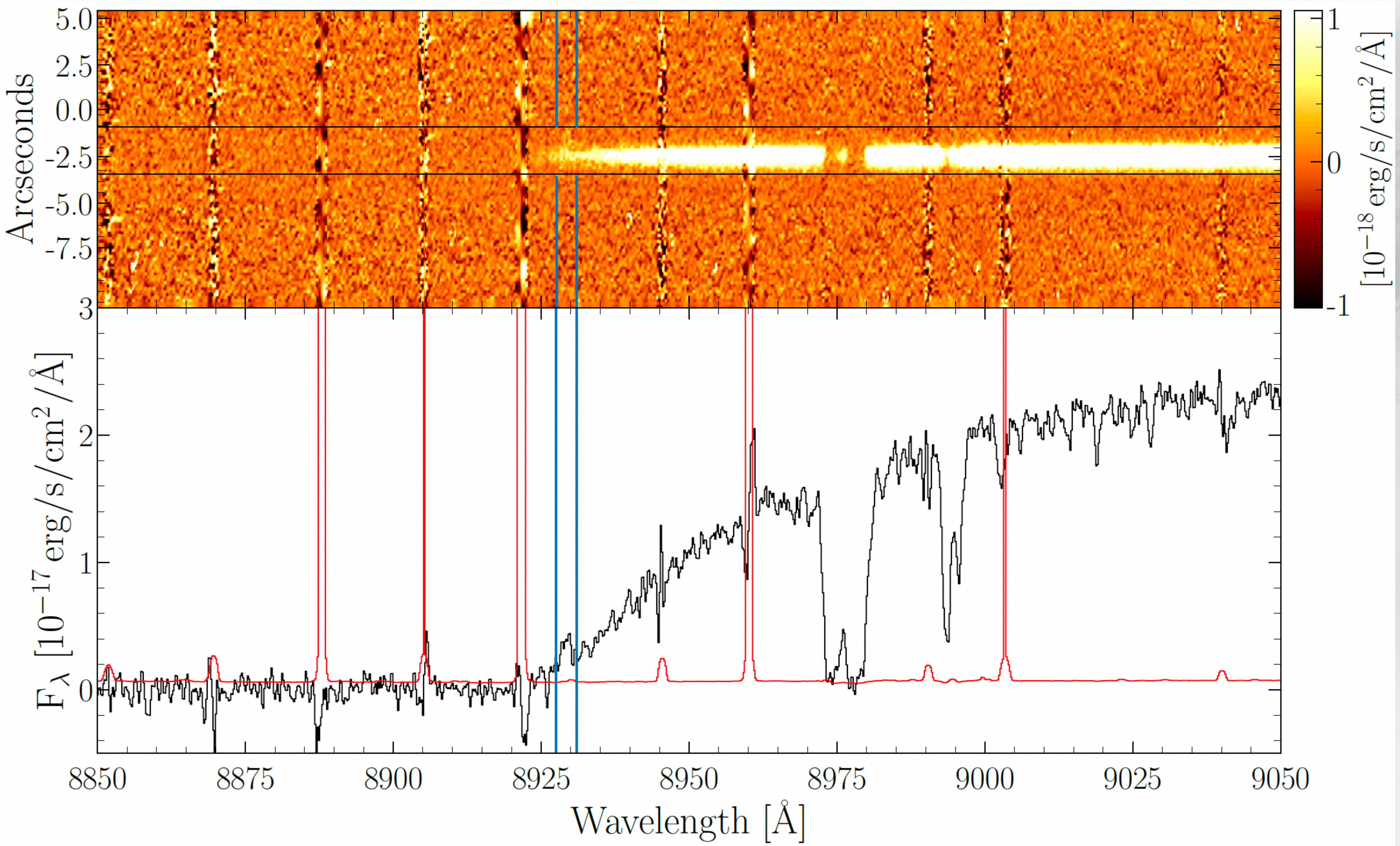

A. Saccardi, S.D. Vergani, A. De Cia et al. 2023 in press

Tentative detection of an emission line at λ 8929Å (observer frame).

$F_{Ly\alpha} = (3.1 \pm 0.6) \times 10^{-18}$ erg s^{-1} cm^{-2}

We tentatively associate it with extended Ly-α emission (covers ~ 2.5″) at z = 6.3449, i.e. ~ 1200 km s^{-1} redward of the DLA

High shift:
Lyα line peak is usually found shifted from the redshift of the host galaxy systemic emission

-Spectroscopic observations revealed Lyα emission at ~ 800 km s^{-1} from the UV galaxy emission lines
(e.g. Hashimoto et al. 2019)

-A shift of a few 100 km s^{-1} is often found between GRB afterglow absorption and emission lines
(e.g. Friis et al. 2015; Vielfaure et al. 2020)

Deep Photometry

Credits: NASA

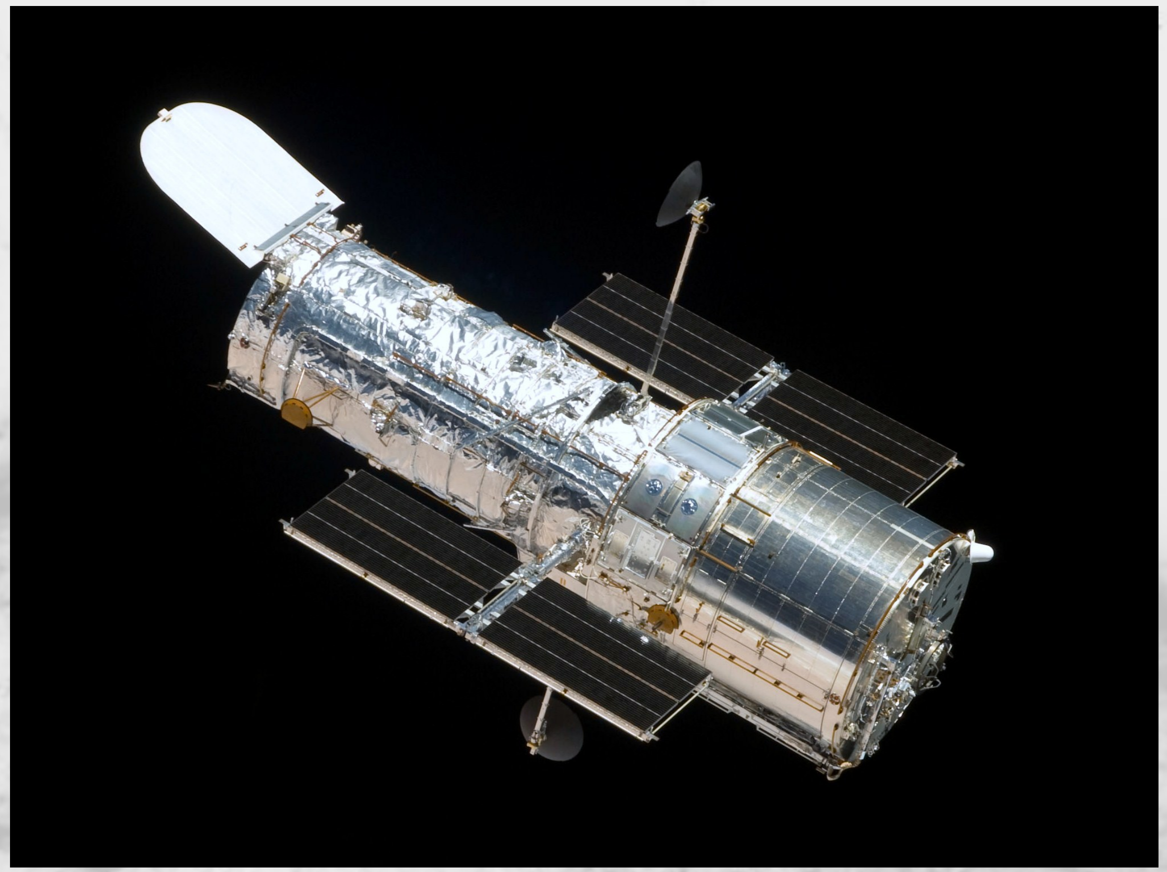

HST

- After ~ 250 days (observer frame)
- 1 exposure of 4800s (IR.F140W)
- Wavelength range 12 000 - 16 000 Å

A. Saccardi, S.D. Vergani, A. De Cia et al. 2023 in press

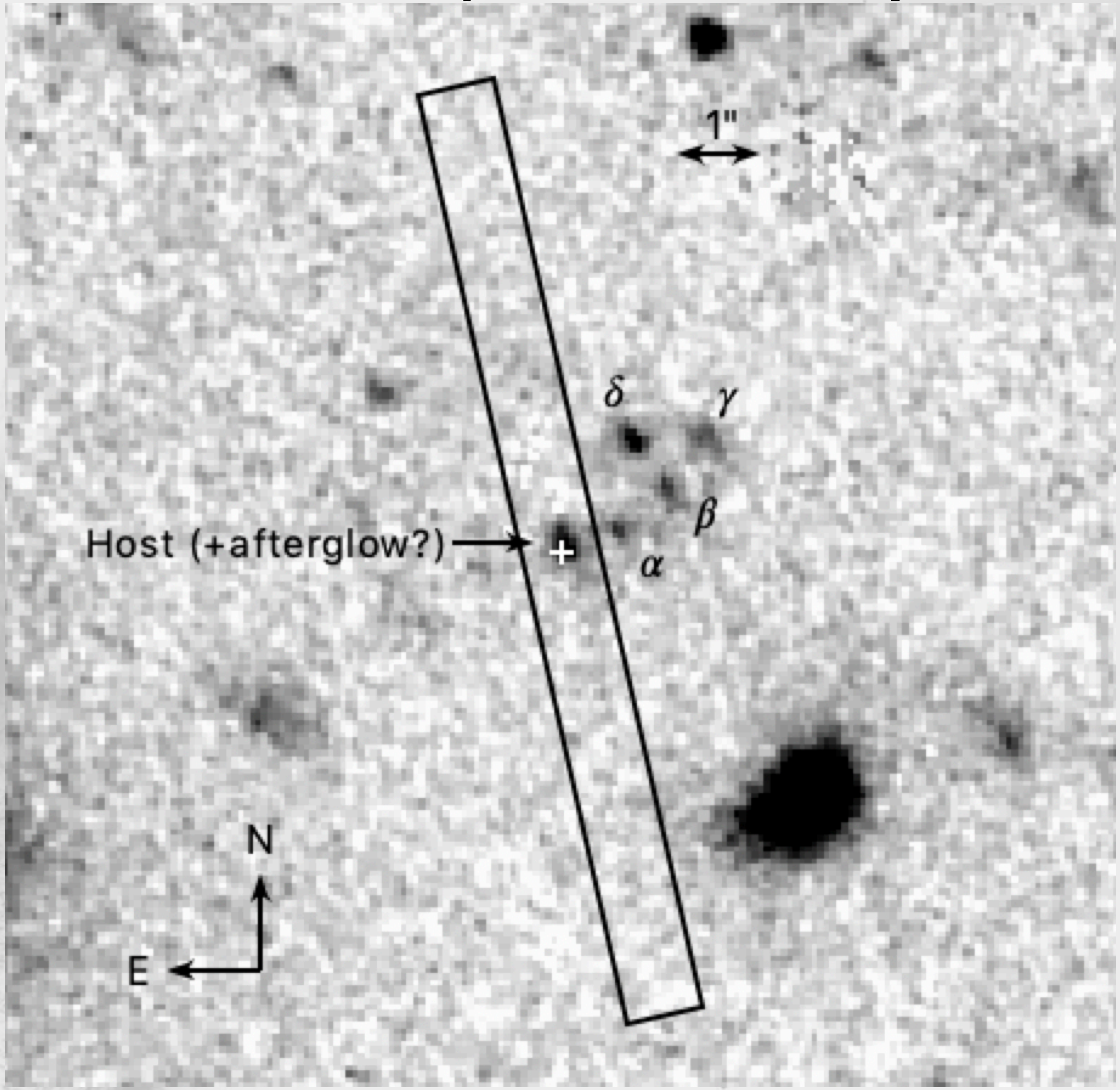

HST/F140W Image

	Projected Distance	Distance z=6.3118
α	0.73″	4.14kpc
β	1.43″	8.14kpc
γ	1.53″	8.67kpc
δ	2.13″	12.08kpc

We have planned another observation in Spring 2023!

FUTURE PERSPECTIVES

VLT/MUSE

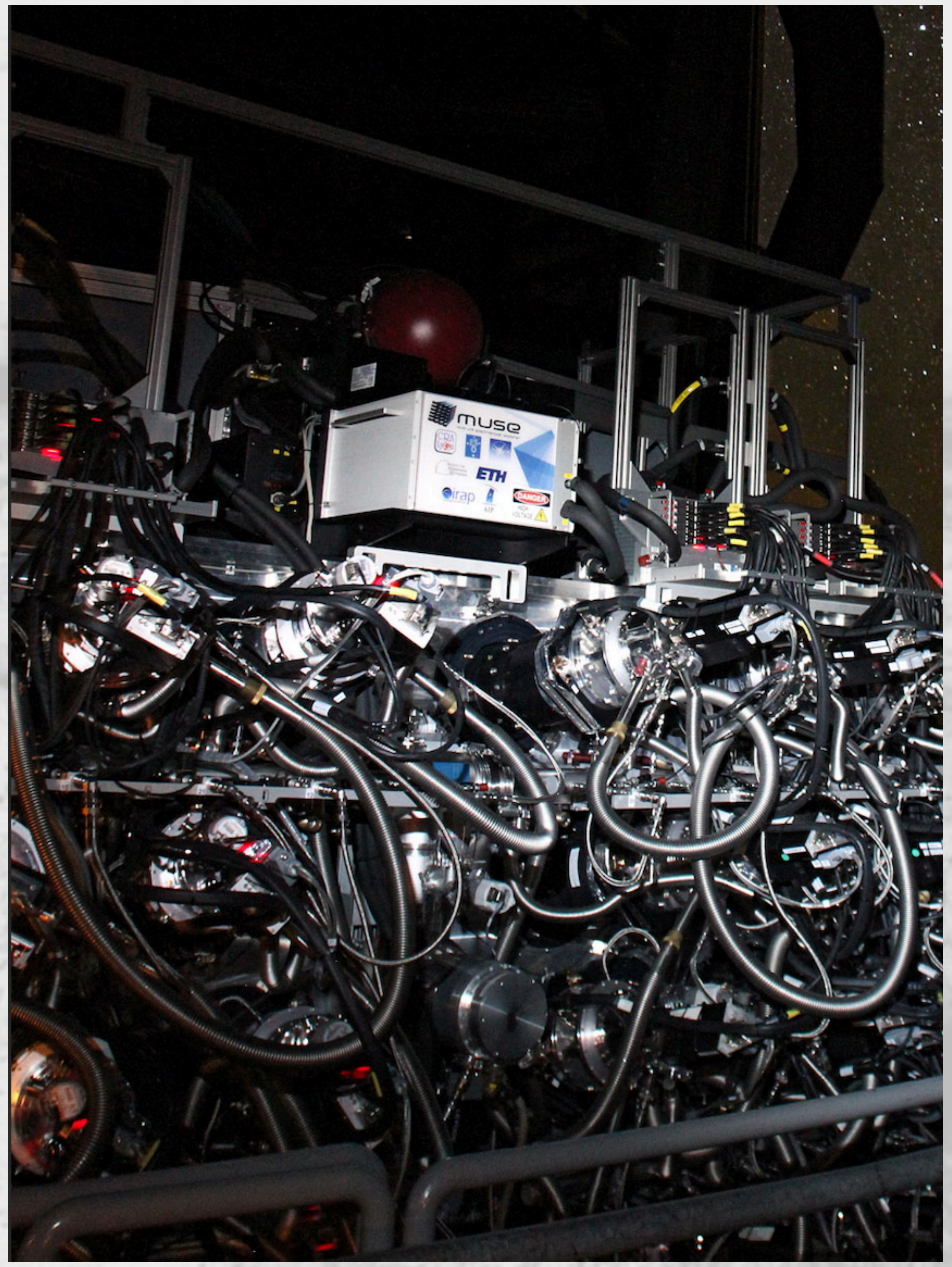

Credits: ESO

Credits: NASA

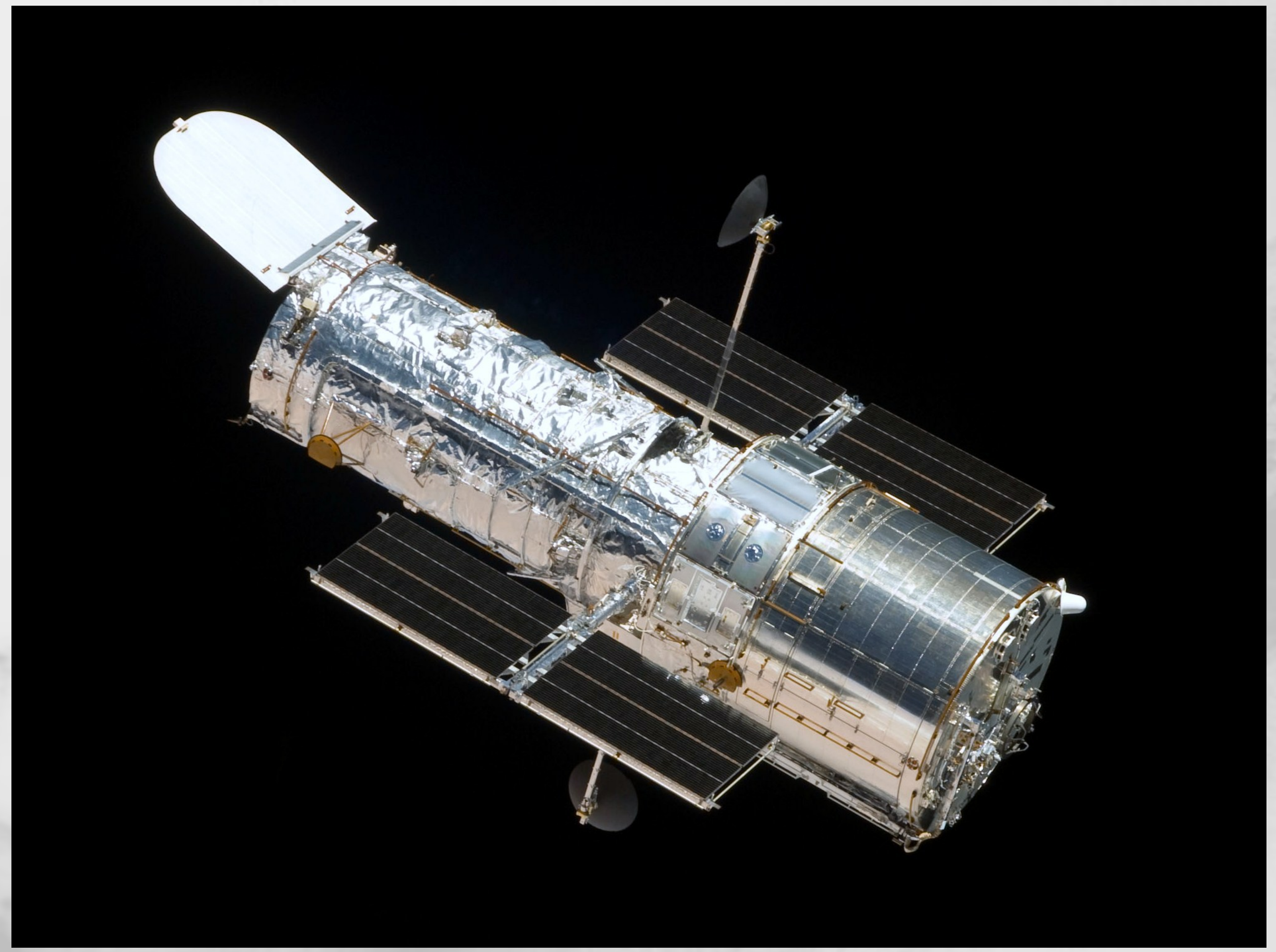

HST

Credits: NASA

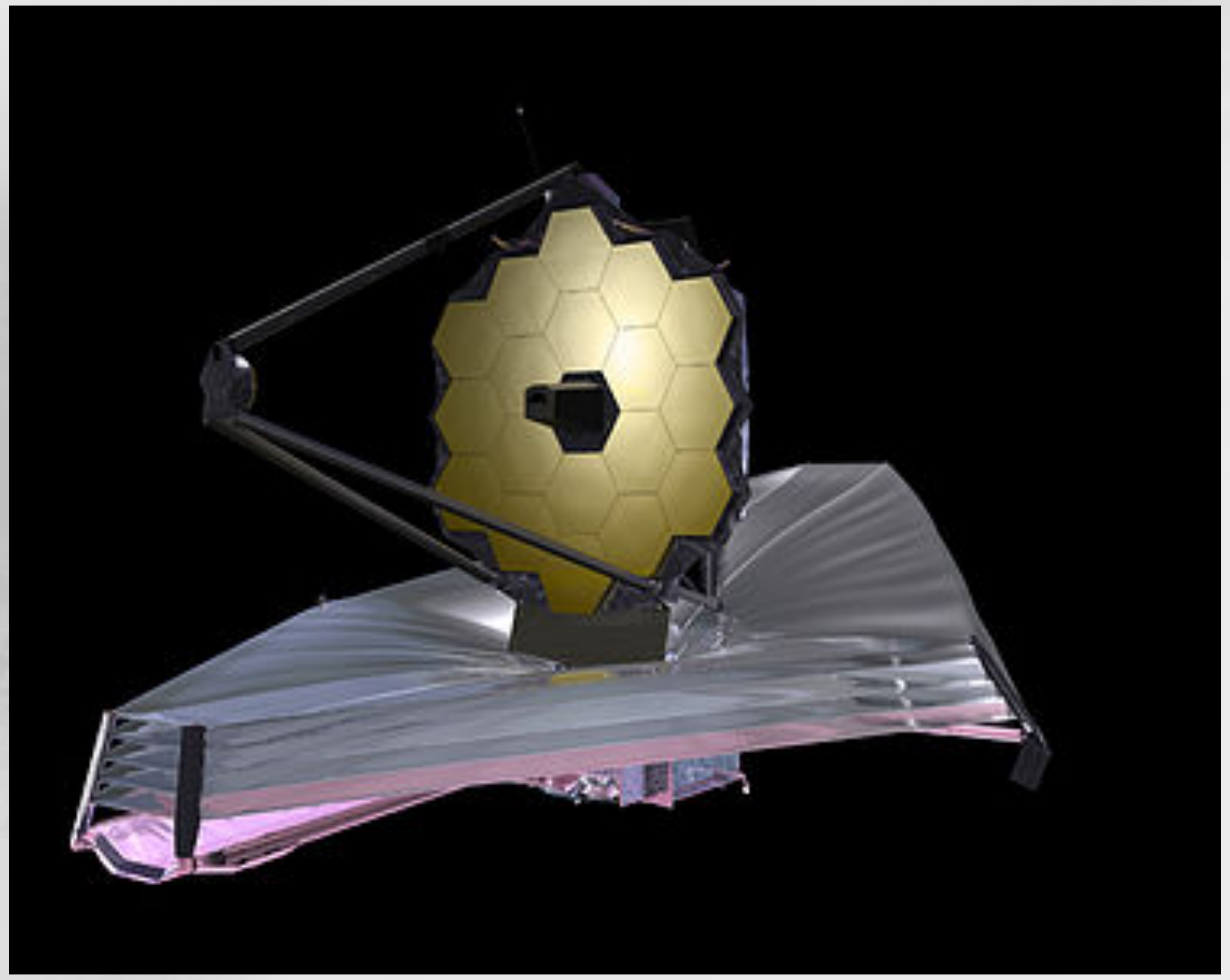

JWST

The properties of the neutral / warm gas (absorption lines)

+

The continuum and ionized gas (emission lines)

FUTURE OBSERVING FACILITIES

SVOM

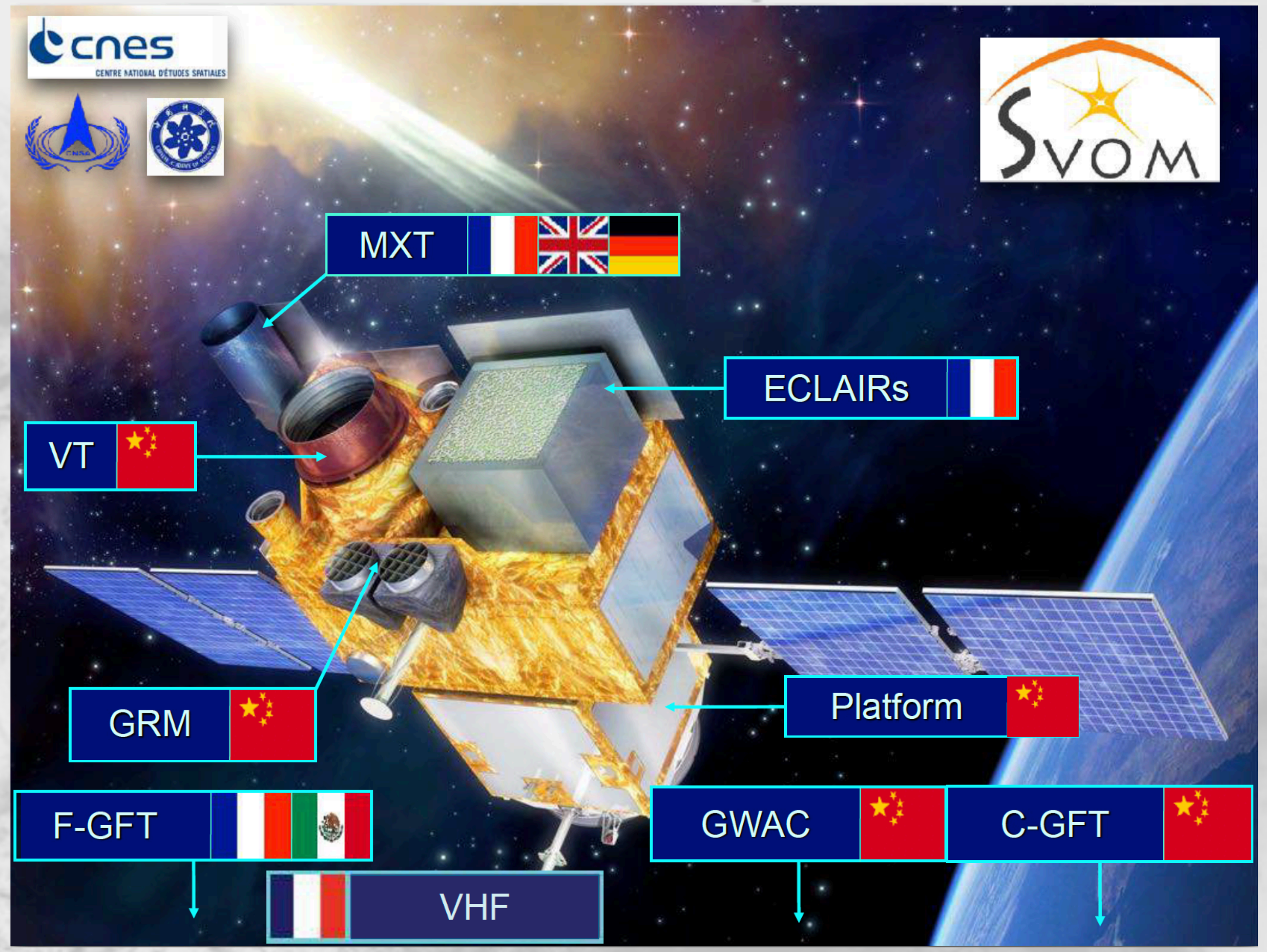

https://www.svom.eu/

Launch December 2023!

See M. Bernardini's Talk

THESEUS

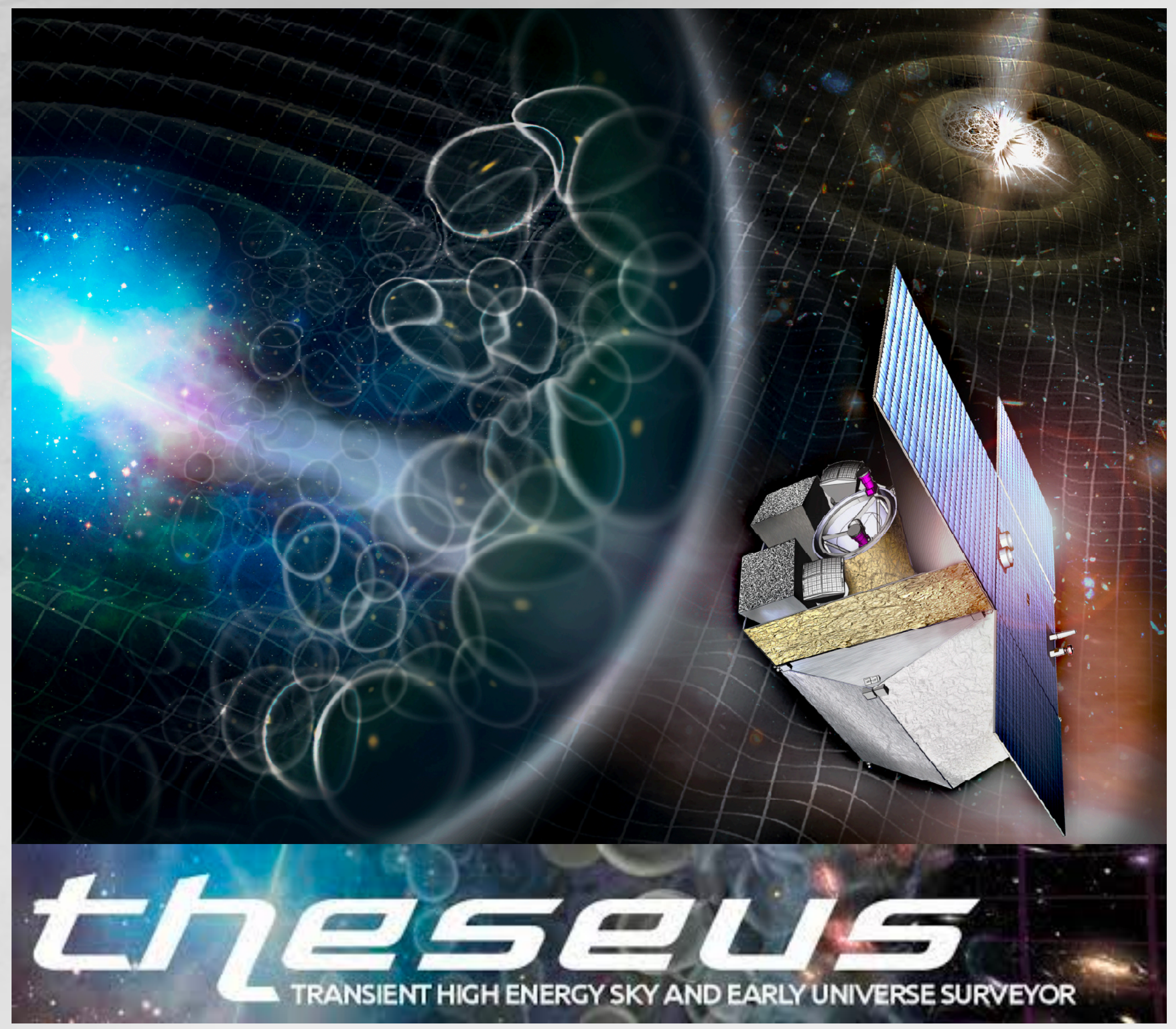

http://www.isdc.unige.ch/theseus

Selected for ESA M7 Phase-0!

See L. Amati's Talk

SEXTEN CENTER FOR ASTROPHYSICS RICCARDO GIACCONI

FUTURE OBSERVING FACILITIES

THESEUS

http://www.isdc.unige.ch/theseus

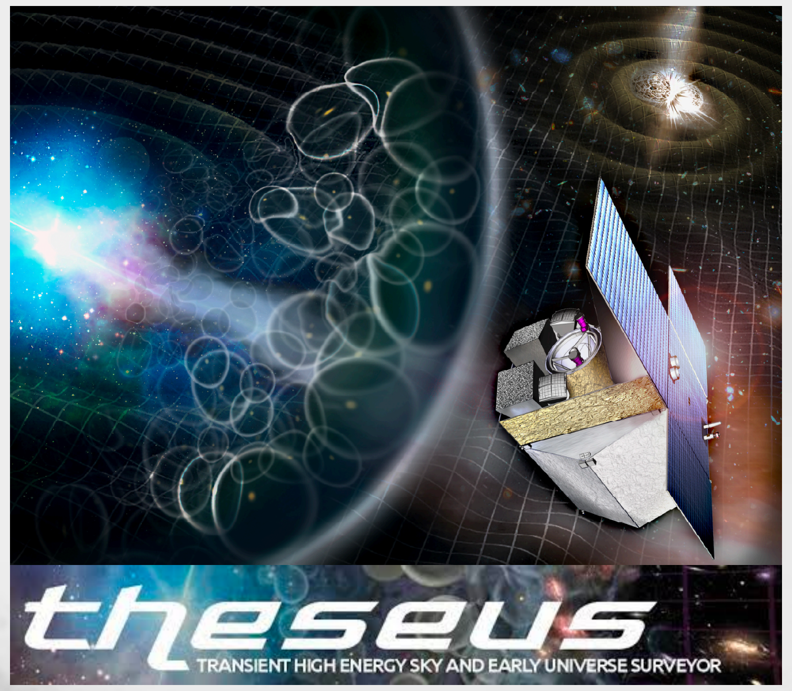

Scientific Objectives:

"Exploring the early Universe with GRBs"

-Global star formation rate from GRB rate as a function of redshift

-The galaxy luminosity function: detecting undetectable galaxies

-The build-up of metals, molecules and dust

-The Lyman-continuum escape fraction

-Did stars reionize the Universe?

-Topology and timeline of Reionization

-Population III stars and primordial galaxies

Payload:

-Soft X-ray Imager (SXI, 0.3 – 5 keV)

-X-Gamma rays Imaging Spectrometer (XGIS, 2 keV – 10 MeV)

-InfraRed Telescope (IRT, 0.7 – 1.8 μm)

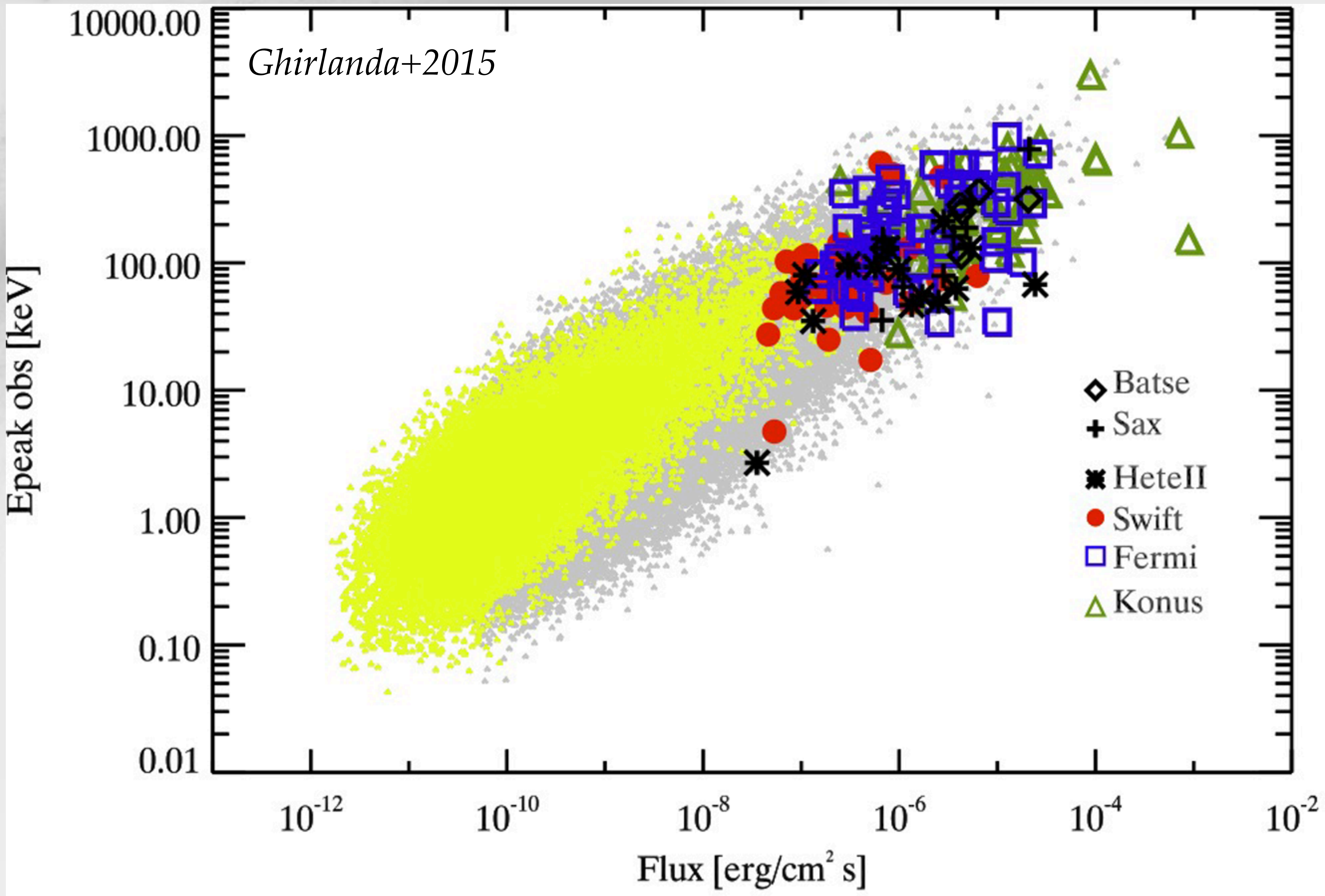

See G. Ghirlanda's Talk

FUTURE OBSERVING FACILITIES

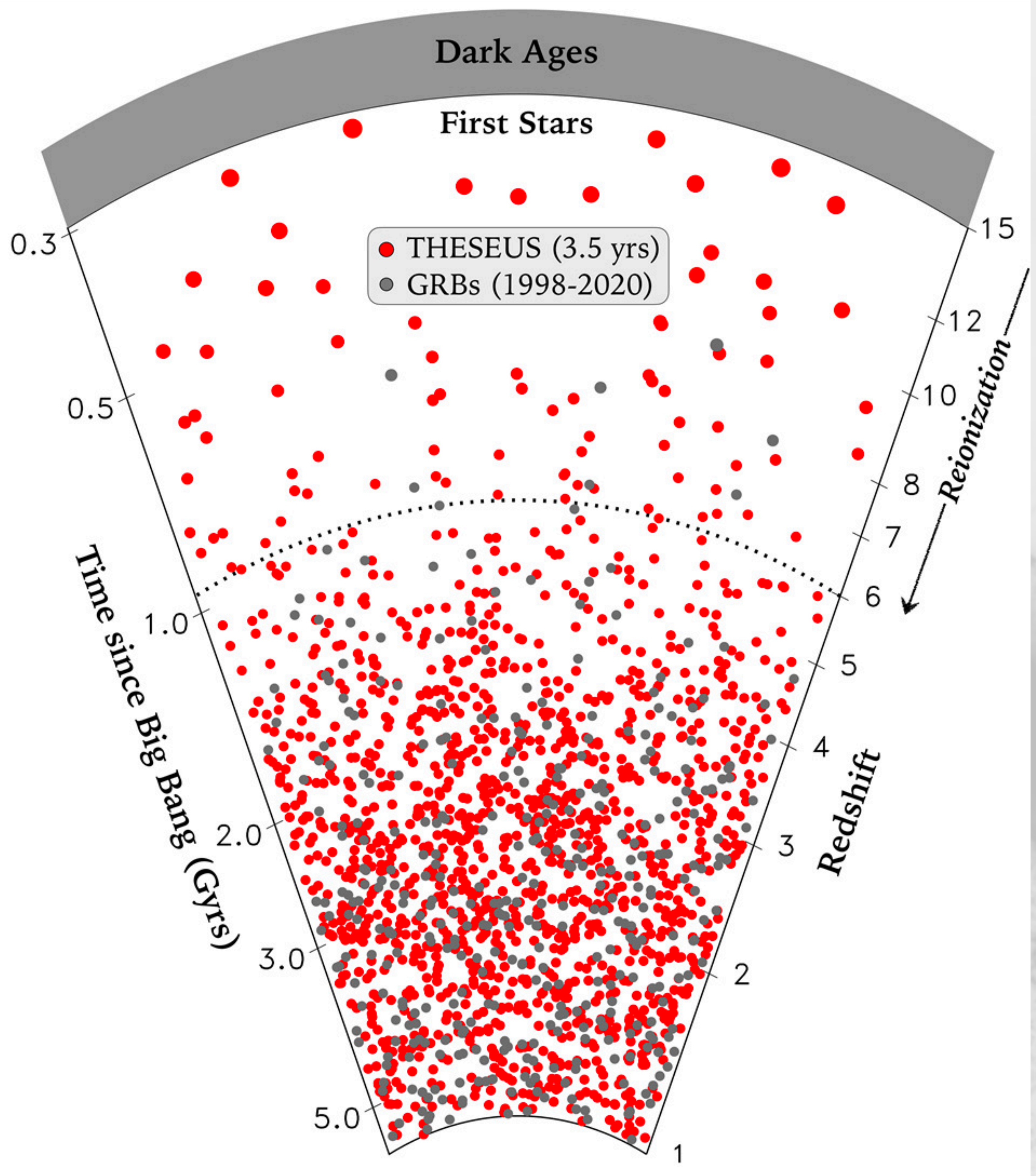

Theseus YB

“The IRT operation sequence after a GRB trigger” (Theseus YB)

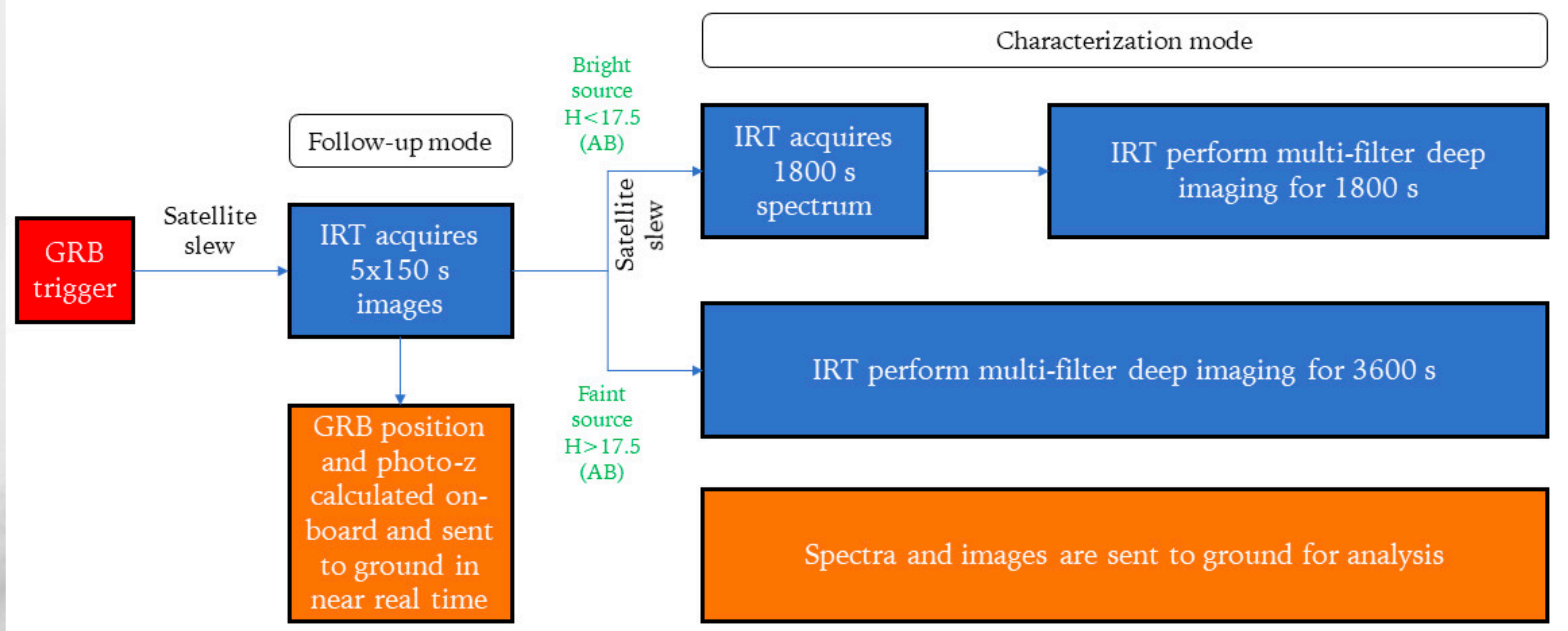

VLT

ELT

CONCLUSIONS

-The formation and evolution of galaxies are key for the current extragalactic astrophysics

-Bright background sources are needed to study the neutral/warm gas

-GRBs are very powerful tools to characterize high redshift galaxies

-Thanks to GRB 210905A we were able to obtain unique and detailed information of the neutral gas and its chemical composition for a galaxy when the Universe was ~0.9 Gyr

-The future is bright thanks to SVOM and we hope THESEUS

THANKS FOR YOUR ATTENTION

HIGH REDSHIFT GAMMA-RAY BURSTS IN THE JWST ERA
9-13 January 2023 - Sexten

SEXTEN CENTER FOR ASTROPHYSICS RICCARDO GIACCONI

ANDREA SACCARDI
2nd year PhD Student
Observatoire de Paris - GEPI
Supervisor: S.D. Vergani

arXiv:2211.16524
In press on A&A

Credits: Futura Science

ED A&A École Doctorale d'Astronomie & Astrophysique d'Ile-de-France

PSL RESEARCH UNIVERSITY PARIS

l'Observatoire de Paris GEPI Galaxies Étoiles Physique et Instrumentation

cnrs

ACAV+

îledeFrance

SVOM

Backup Slides

Credits: Futura Science

$[M/H]_{TOT}$

The dust-corrected (total of gas and dust) abundances can defined as

$$[X/\mathrm{H}]_{\mathrm{tot}} = [X/\mathrm{H}] - \delta_X,$$

where [X/H] is the observed abundance of metal X and δ_X is its depletion in dust

A dust tracer can be [Zn/Fe].
Assuming a certain slope for the expected depletion:

$$\delta_X = A2_X + B2_X \times [\mathrm{Zn/Fe}],$$

$$y = a + bx,$$

$$a = [\mathrm{M/H}]_{\mathrm{tot}},$$

$$b = [\mathrm{Zn/Fe}]_{\mathrm{fit}},$$

$$x = B2_X,$$

$$y = \log N(X) - X_{\odot} + 12. - A2_X - \log N(\mathrm{H})$$

SEXTEN CENTER FOR ASTROPHYSICS RICCARDO GIACCONI

Table A.3: [X/Fe] residuals of the depletion pattern fitting (see Figs. 7, A.4 and A.5). The values and uncertainties are obtained including MC simulations to take into account the dust depletion errors. We stress that the impact of dust depletion on the nuclear abundances is correlated between elements; i.e., a higher dust depletion correction lowers all [X/Fe] values except for [Al/Fe] which it raises, and vice-versa.

With α-element corr.	I	II	III	IV	V	VI	Tot
[C/Fe]	$0.73^{+0.06}_{-0.09}$	$-0.41^{+0.10}_{-0.10}$	$0.20^{+0.16}_{-0.16}$	$0.44^{+0.09}_{-0.14}$	$0.36^{+0.12}_{-0.18}$	$0.10^{+0.12}_{-0.12}$	$0.29^{+0.10}_{-0.10}$
[O/Fe]	$0.35^{+0.06}_{-0.09}$	$0.04^{+0.09}_{-0.10}$	$-0.33^{+0.15}_{-0.15}$	$-0.28^{+0.09}_{-0.13}$	$-0.60^{+0.11}_{-0.16}$	$-0.42^{+0.11}_{-0.11}$	$0.07^{+0.09}_{-0.09}$
[Mg/Fe]	$0.13^{+0.03}_{-0.05}$	$0.69^{+0.05}_{-0.05}$	$0.35^{+0.08}_{-0.08}$	$0.32^{+0.05}_{-0.07}$	$0.30^{+0.06}_{-0.09}$	$-0.61^{+0.06}_{-0.06}$	$0.40^{+0.05}_{-0.05}$
[Al/Fe]	$0.29^{+0.03}_{-0.02}$	$0.74^{+0.04}_{-0.04}$	$0.95^{+0.06}_{-0.06}$	$1.07^{+0.05}_{-0.03}$			$0.45^{+0.04}_{-0.04}$
[Si/Fe]	$0.28^{+0.03}_{-0.04}$	$0.37^{+0.05}_{-0.05}$	$0.50^{+0.07}_{-0.07}$	$0.32^{+0.04}_{-0.06}$	$0.20^{+0.05}_{-0.08}$	$0.34^{+0.05}_{-0.05}$	$0.34^{+0.05}_{-0.05}$
[S/Fe]	$0.26^{+0.04}_{-0.06}$	$0.28^{+0.07}_{-0.07}$	$1.05^{+0.11}_{-0.11}$				$0.28^{+0.07}_{-0.07}$
Without α-element corr.	I	II	III	IV	V	VI	Tot
[C/Fe]	$0.31^{+0.13}_{-0.13}$	$-0.97^{+0.13}_{-0.13}$	$-0.24^{+0.17}_{-0.17}$	$0.29^{+0.16}_{-0.18}$	$0.00^{+0.21}_{-0.22}$	$-0.59^{+0.16}_{-0.16}$	$-0.36^{+0.14}_{-0.14}$
[O/Fe]	$-0.04^{+0.12}_{-0.12}$	$-0.47^{+0.12}_{-0.12}$	$-0.74^{+0.16}_{-0.16}$	$-0.42^{+0.15}_{-0.17}$	$-0.93^{+0.20}_{-0.20}$	$-1.05^{+0.15}_{-0.15}$	$-0.52^{+0.13}_{-0.13}$
[Mg/Fe]	$-0.09^{+0.07}_{-0.07}$	$0.40^{+0.07}_{-0.07}$	$0.12^{+0.09}_{-0.09}$	$0.25^{+0.08}_{-0.10}$	$0.11^{+0.11}_{-0.11}$	$-0.96^{+0.08}_{-0.08}$	$0.07^{+0.07}_{-0.07}$
[Al/Fe]	$0.44^{+0.04}_{-0.04}$	$0.93^{+0.04}_{-0.04}$	$1.10^{+0.06}_{-0.06}$	$1.12^{+0.06}_{-0.06}$			$0.68^{+0.05}_{-0.05}$
[Si/Fe]	$0.10^{+0.06}_{-0.06}$	$0.12^{+0.06}_{-0.06}$	$0.31^{+0.08}_{-0.08}$	$0.26^{+0.07}_{-0.08}$	$0.04^{+0.09}_{-0.10}$	$0.04^{+0.07}_{-0.07}$	$0.06^{+0.06}_{-0.06}$
[S/Fe]	$-0.03^{+0.09}_{-0.09}$	$-0.10^{+0.09}_{-0.09}$	$0.75^{+0.12}_{-0.12}$				$-0.16^{+0.09}_{-0.09}$

$[M/H]_{TOT}$ and DTM

Table 6: Properties derived from the total metal abundances and component by component. The total metallicity ($[M/H]_{tot}$), dust depletion $[Zn/Fe]_{fit}$ and dust-to-metal ratio (DTM) are reported for the analysis performed taking α-element enhancement into account.

With α-element corr.	I	II	III	IV	V	VI	Tot
$[M/H]_{tot}$							-1.72 ± 0.13
$[Zn/Fe]_{fit}$	$0.00^{+0.11}_{-0.00}$	$0.53^{+0.09}_{-0.09}$	$0.57^{+0.14}_{-0.14}$	$0.00^{+0.17}_{-0.00}$	$0.00^{+0.21}_{-0.00}$	$0.53^{+0.10}_{-0.10}$	0.33 ± 0.09
DTM	$0.00^{+0.04}_{-0.00}$	$0.26^{+0.03}_{-0.03}$	$0.27^{+0.04}_{-0.04}$	$0.00^{+0.06}_{-0.00}$	$0.00^{+0.07}_{-0.00}$	$0.26^{+0.03}_{-0.03}$	0.18 ± 0.03

$[M/H]_{TOT}$ and DTM - no alpha element enhancement

Table A.1: Properties derived from the total metal abundances and component by component. The total metallicity ($[M/H]_{tot}$), dust depletion $[Zn/Fe]_{fit}$, dust-to-metal ratio (DTM) and dust extinction (A_V (mag)) are reported for the analysis performed not taking α-element enhancement into account.

Without α-element corr.	*I*	*II*	*III*	*IV*	*V*	*VI*	Tot
$[M/H]_{tot}$							-1.01 ± 0.14
$[Zn/Fe]_{fit}$	$0.44^{+0.11}_{-0.11}$	$1.01^{+0.11}_{-0.11}$	$0.95^{+0.15}_{-0.15}$	$0.22^{+0.17}_{-0.17}$	$0.45^{+0.19}_{-0.19}$	$1.12^{+0.14}_{-0.14}$	0.89 ± 0.12
DTM	$0.23^{+0.03}_{-0.03}$	$0.38^{+0.04}_{-0.04}$	$0.37^{+0.04}_{-0.04}$	$0.13^{+0.04}_{-0.04}$	$0.23^{+0.04}_{-0.04}$	$0.41^{+0.05}_{-0.05}$	0.36 ± 0.04
A_V (mag)							0.04 ± 0.02

Observed Metal Abundances

Table 5: Metal abundances. For each element (first column), the total column density (second column), the ratio over iron (third column) and the metallicity are reported.

X	$\log(N/\mathrm{cm}^{-2})$	$[X/\mathrm{Fe}]$	[X/H]
C	> 16.02	> 0.66	> -1.5
O	> 16.03	> 0.41	> -1.8
Mg	> 15.13	> 0.61	> -1.6
Al	> 13.69	> 0.31	> -1.8
Si	14.90 ± 0.02	0.46 ± 0.04	-1.71 ± 0.11
S	> 14.50	> 0.45	> -1.7
Fe	14.43 ± 0.02		-2.17 ± 0.11

Column Densities

$\log N_{HI} = 21.10 +/- 0.1$

Table 2: Column density of low ionization lines. The velocity shift of the components with respect to the N v line is indicated. The last row reports the Doppler parameter *b* of each component as resolved by the X-shooter observations.

Species	*I*	*II*	*III*	*IV*	*V*	*VI*
Velocity	-255 km s^{-1}	-203 km s^{-1}	-136 km s^{-1}	-25 km s^{-1}	$+46$ km s^{-1}	$+75$ km s^{-1}
C II λ1334	> 15.79	> 15.02	> 14.35	> 14.30	> 14.72	> 15.33
C II* λ1335					13.16 ± 0.17	13.43 ± 0.09
O I λ1302	> 15.66	> 15.68	14.02 ± 0.12	13.83 ± 0.18	> 14.01	> 15.02
Mg II λ2796, λ2803§	> 14.32	> 15.01	> 13.36	> 13.30	> 13.76	> 13.51
Al II λ1670‡	> 13.25	> 13.37	> 12.23	> 12.77		
Si II λ1260, λ1304, λ1808	14.33 ± 0.04	14.50 ± 0.03	13.32 ± 0.05	13.15 ± 0.03	13.51 ± 0.07	14.27 ± 0.02
Si II* λ1264		12.76 ± 0.04	12.49 ± 0.08		12.02 ± 0.09	12.44 ± 0.07
S II λ1259†	13.99 ± 0.09	14.22 ± 0.09	13.69 ± 0.09			
Fe II λ1608, λ2344, λ2382	14.03 ± 0.04	13.88 ± 0.02	12.55 ± 0.09	12.79 ± 0.09	13.26 ± 0.04	13.68 ± 0.02
b (km s^{-1})	15.6	27.7	21.7	28.4	29.6	23.2

§ Mg II lines are particularly uncertain because they are found in a very noisy region at the end of the NIR arm spectrum.

‡ The *V*, *VI* (and partially *IV*) components of Al II are strongly affected by a sky line and could not be determined.

† The *IV*, *V*, *VI* components of S II are blended with the Si II λ1260 Å absorption.

Table 3: Column density of high ionization lines. The velocity shift of the components with respect to the N v line are indicated. The last row reports the Doppler parameter *b* used of each component as resolved by the X-shooter observations.

Species	1	2	3	4
Velocity	-220 km s^{-1}	-72 km s^{-1}	0 km s^{-1}	$+71$ km s^{-1}
C IV λ1548, λ1550	> 14.36	> 14.13	> 16.2	> 14.08
N V λ1238, λ1242			> 14.25	
Si IV λ1393, λ1402	> 13.89	> 13.41	> 13.82	> 13.63
b (km s^{-1})	56.2	46.0	15.5	31.2

HST Magnitudes

F140W magnitude is 25.66 ± 0.05 mag (AB), corresponding to $SFR_{UV} \sim 20\ M_{\odot}\ yr^{-1}$ (see Rossi et al. 2022)

A. Saccardi, S.D. Vergani, A. De Cia et al. 2023 in press

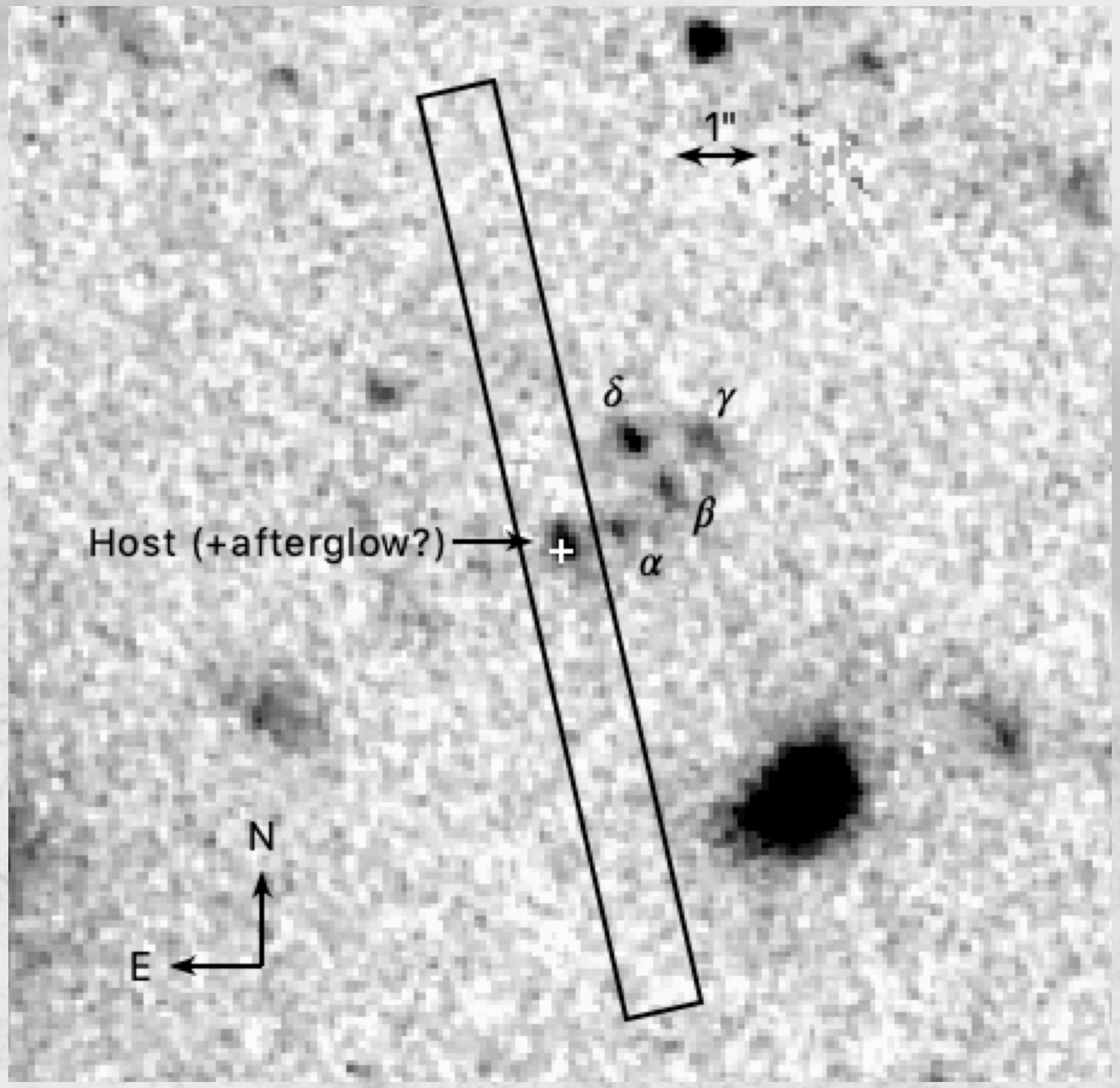

The F140W magnitudes of the single objects are

α 26.46 ± 0.07 mag (AB)
β 26.38 ± 0.06 mag (AB)
γ 26.34 ± 0.06 mag (AB)
δ 25.98 ± 0.05 mag (AB)